HHS Public Access

Author manuscript

Cell Rep. Author manuscript; available in PMC 2024 July 15.

Published in final edited form as:

Cell Rep. 2024 June 25; 43(6): 114288. doi:10.1016/j.celrep.2024.114288.

G-protein-coupled receptor 84 regulates acute inflammation in normal and diabetic skin wounds

Paula O. Cooper[1], **Sarah S. Kleb**[1], **Satish K. Noonepalle**[1], **Veronica M. Amuso**[1], **Rohan Varshney**[2], **Michael C. Rudolph**[2], **Tanvir K. Dhaliwal**[1], **Darlene V. Nguyen**[1], **Miguel F. Mazumder**[1], **Najuma S. Babirye**[1], **Ruchi Gupta**[3], **Bao-Ngoc Nguyen**[1,3], **Brett A. Shook**[1,4,5,*]

[1]Department of Biochemistry and Molecular Medicine, School of Medicine and Health Sciences, The George Washington University, Washington, DC 20037, USA

[2]Department of Biochemistry and Physiology, The University of Oklahoma Health Sciences Center, Oklahoma City, OK 73104, USA

[3]Department of Surgery, School of Medicine and Health Sciences, The George Washington University, Washington, DC 20037, USA

[4]Department of Dermatology, School of Medicine and Health Sciences, The George Washington University, Washington, DC 20037, USA

[5]Lead contact

SUMMARY

Lipids have emerged as potent regulators of immune cell function. In the skin, adipocyte lipolysis increases the local pool of free fatty acids and is essential for coordinating early macrophage inflammation following injury. Here, we investigate G-protein-coupled receptor 84 (GPR84), a medium-chain fatty acid (MCFA) receptor, for its potential to propagate pro-inflammatory signaling after skin injury. GPR84 signaling was identified as a key component of regulating myeloid cell numbers and subsequent tissue repair through *in vivo* administration of a pharmacological antagonist and the MCFA decanoic acid. We found that impaired injury-induced dermal adipocyte lipolysis is a hallmark of diabetes, and lipidomic analysis demonstrated that MCFAs are significantly reduced in diabetic murine wounds. Furthermore, local administration of decanoic acid rescued myeloid cell numbers and tissue repair during diabetic wound healing. Thus, GPR84 is a readily targetable lipid signaling pathway for manipulating injury-induced tissue inflammation with beneficial effects on acute diabetic healing.

*Correspondence: brettshook@gwu.edu.

AUTHOR CONTRIBUTIONS

Conceptualization, P.O.C. and B.A.S.; methodology, P.O.C., M.C.R., and B.A.S.; formal analysis, P.O.C., S.S.K., T.K.D., D.V.N., and B.A.S.; investigation, P.O.C., S.K.N., V.M.A., M.F.M., N.S.B., R.V., S.S.K., M.C.R., T.K.D., D.V.N., and R.G.; resources, M.C.R., B.-N.N., and B.A.S.; writing – original draft, P.O.C. and B.A.S.; writing – review & editing, P.O.C. and B.A.S.; supervision, M.C.R., P.O.C., and B.A.S.; funding acquisition, M.C.R. and B.A.S.

SUPPLEMENTAL INFORMATION

Supplemental information can be found online at https://doi.org/10.1016/j.celrep.2024.114288.

DECLARATION OF INTERESTS

The authors have no competing interests.

Graphical abstract

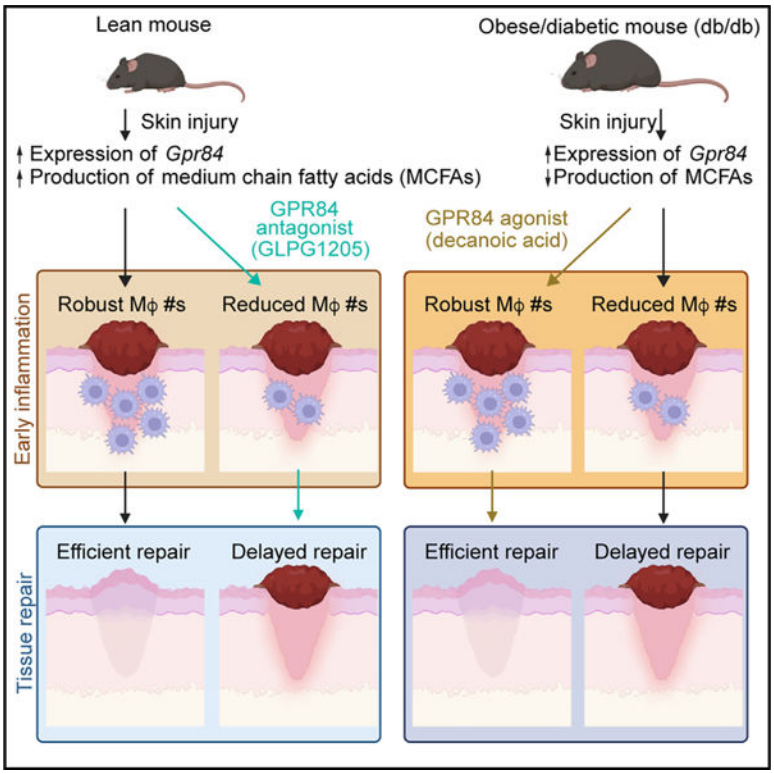

In brief

Using pharmacological approaches during mouse skin wound healing, Cooper et al. show that GPR84 signaling contributes to myeloid cell numbers during inflammation. While inhibiting GPR84 signaling delays wound healing in lean, young mice, the administration of a GPR84 agonist rescues impaired myeloid cell recruitment and subsequent wound healing in diabetic mice.

INTRODUCTION

The injury response is an intricate process that must proceed rapidly and efficiently to restore tissue function. Robust early inflammation recruits and supports pro-inflammatory neutrophils and macrophages to clear cellular debris and pathogens.[1,2] Then, a complex multicellular response changes the local environment from pro-inflammatory to a pro-healing cellular state, initiating reparative processes during the proliferation phase of wound healing.[1–3] During the proliferation phase, epithelial cell migration and division close the wound, while fibroblasts and endothelial cells produce new dermal tissue that is later matured.[4–6] Activation and recruitment of the innate immune system are essential for efficient progression through the wound-healing process,[7–9] and fluctuations in the immune response are associated with impaired wound healing that is observed with diabetes and aging.[10–15]

Robust pro-inflammatory signals promote the rapid accumulation of neutrophils, monocytes, and pro-inflammatory macrophages during early wound healing.[2,16,17] Ample numbers of

macrophages must be recruited to the site of injury during inflammation, as models with reduced inflammation-phase macrophage numbers result in delayed wound healing.[18–21] As the inflammation phase progresses, macrophage numbers are maintained, while their gene expression profile changes from the production of pro-inflammatory to pro-healing factors that are essential for efficient tissue repair.[16,22–25] While macrophage recruitment and polarization are regulated by numerous tissue-resident cells including keratinocytes and adipocytes, the complete underpinning mechanisms are not clearly defined. Given that altered macrophage responses are central to delayed healing associated with numerous pathologies,[1,26] there is a critical need to identify targetable mechanisms that influence macrophages under pathological conditions.

Recently, we have shown that dermal adipocytes break down their stored triglycerides (TGs) into free fatty acids (FFAs) following injury.[27] While blocking injury-induced adipocyte lipolysis results in decreased inflammation-phase macrophages and delays revascularization, the molecular mechanism connecting lipid breakdown to macrophage infiltration is poorly understood. When adipocyte lipolysis is blocked during skin wound healing, the abundance of medium-chain fatty acids (MCFAs) is significantly reduced.[27] Interestingly, MCFAs bind to the G-protein-coupled receptor 84 (GPR84) to promote myeloid cell migration, phagocytosis, and expression of pro-inflammatory factors such as tumor necrosis factor alpha (TNF-α), interleukin (IL)-8, and IL-12.[28–31] Increased myeloid cell GPR84 expression and signaling during inflammation supports macrophage cell numbers in the liver and further promotes pro-inflammatory processes such as NLRP3 inflammasome activation in the large intestine, alveolar macrophage activation in the lungs, and microglial motility in the brain.[32–38] Additionally, GPR84 RNA and protein levels are elevated in multiple organs in murine models of diabetes and fibrosis[36,37] and contribute to inflammatory diseases such as gastroesophageal reflux disease, ulcerative colitis, and acute respiratory distress syndrome.[39–42] Not only is GPR84 conserved across mammalian species to promote inflammation,[31] but silencing of the GPR84 homolog in *Drosophila* prevents hemocytes from extravasating from vessels to wounds.[43] While the inhibition of GPR84 signaling reduces fibrosis in murine models in the lung, heart, kidney, liver, pancreas, and skin,[32,37,38] whether GPR84 plays a role in skin wound inflammation remains unknown.

Herein, we explored GPR84 signaling in the context of acute inflammation following injury by manipulating GPR84 signaling *in vivo* with systemic administration of a selective functional antagonist (GLPG1205) and local injections of an agonist (decanoic acid [DA]).[30,44] We found that GPR84 inhibition reduced myeloid cell numbers during the inflammation phase of skin wound healing. When we assessed subsequent tissue repair, we observed defects in revascularization, re-epithelialization, and fibroblast repopulation 7 days post-wounding (DPW). Since these features are characteristic of delayed diabetic wound healing,[16,45,46] we examined diabetic mouse (db/db) skin wounds for their capacity to activate GPR84. We detected impaired injury-stimulated adipocyte lipolysis, reduced wound-associated MCFAs, and reduced macrophage numbers in diabetic mice. Interestingly, the administration of DA rescued pro-inflammatory myeloid cell numbers in diabetic mouse wounds 2 DPW and improved revascularization and wound closure 7 DPW. These findings reveal a vital role for GPR84 signaling in myeloid cell inflammation during the early stages

of skin wound inflammation and demonstrate that activating this pathway can improve repair in diabetic mice.

RESULTS

GPR84 is expressed by myeloid and stromal cells during the inflammation phase of skin wound healing

GPR84 signaling contributes to tissue inflammation in the brain, lungs, kidney, and digestive system[30,38,40]; however, its expression patterns and involvement in cutaneous inflammation have not been explored. To investigate GPR84 expression in uninjured skin and during the inflammation phase following injury, we isolated multiple cell populations and performed gene expression analysis (Figures S1A and S1B). Macrophages isolated from uninjured skin were enriched for *Gpr84* expression compared to the total stromal vascular fraction (SVF) of uninjured skin (Figure 1A). Myeloid cells (macrophages, monocytes, and neutrophils) isolated from skin 1.5 DPW showed a greater expression of *Gpr84* (Figure 1A), consistent with other reports demonstrating increased *Gpr84* expression in pro-inflammatory myeloid cells.[30,36,47] Since increased expression or signaling through GPR84 has been demonstrated in adipocytes, fibroblasts/mesenchymal cells, and epithelial cells, we extended our analysis to include these cellular subsets in the skin (Figure 1A). While these cell populations did not have enriched expression of *Gpr84* when isolated from uninjured skin, *Gpr84* expression was increased 40-fold in adipocytes and 20-fold in total mesenchymal cells (CD45, CD31, and EpCAM lineage negative [Lin–]) (Figure 1A). We confirmed that our adipocyte isolations were not contaminated with immune cells by demonstrating a lack of *Ptprc* (CD45) expression in our adipocyte samples compared to the uninjured skin SVF (Figure S1C) and fluorescence-activated cell sorting-isolated Lin– cells isolated from 1.5 DPW tissue (Figure S1D). While keratinocytes from 1.5 DPW tissue showed greater expression of *Gpr84* than keratinocytes from uninjured skin, the level of expression was still lower than *Gpr84* expression of the SVF from uninjured skin (Figure 1A). These data indicate that tissue-resident stromal cells express *Gpr84* after injury and are consistent with evidence that non-immune cells contribute to the tightly coordinated immune response during skin wound healing.[5,48,49] Taken together, these data reveal that *Gpr84* levels increase in various cutaneous cell populations following acute injury, implicating GPR84 signaling as a potential contributor to the skin injury response.

GPR84 signaling regulates myeloid cell numbers during the inflammation phase of skin wound healing

Since multiple cell types express *Gpr84* during the inflammatory phase of skin wound healing, we sought to determine whether GPR84 signaling contributes to the inflammation phase of repair. Selective agonists and antagonists have been developed to manipulate GPR84 signaling. In particular, 6-(octylamino)-2,4(1H,3H)-pyrimidinedione is a synthetic selective agonist, and DA is a naturally occurring MCFA that activates GPR84.[28,29,31,35] These agonists can increase myeloid cell migration, pro-inflammatory gene expression (Figure S1E), and phagocytosis *in vitro*.[36,50,51] Furthermore, the GPR84-mediated effect of these agonists can be blocked with the selective functional antagonist GLPG1205 (Figure S1F).[42,52] To determine whether GPR84 has a functional role during skin wound healing,

mice were fed 30 mg/kg GLPG1205 twice daily, from 1 day prior to wounding until 2 days after injury, to inhibit GPR84 signaling (Figure 1B).[52] We then examined the effect of GLPG1205 on the composition of myeloid cells using flow cytometry to identify total immune cells ($CD45^+$), monocytes ($CD45^+$, $CD11b^+$, $F4/80^-$), macrophages ($CD45^+$, $CD11b^+$, $F4/80^+$), and neutrophils ($CD45^+$, $Ly6G^+$) (Figure S1A).[23,27] Additionally, macrophage polarization was assessed using Ly6C and CD206 to identify pro-inflammatory and pro-healing macrophages, respectively.[23,24,53–57] While GLPG1205 caused no reduction in the abundance of myeloid cell subsets in non-wounded (NW) skin, bone marrow, blood, spleen, liver, or visceral white adipose tissue (Figures S2A–S2F), we observed a 30% reduction in $CD45^+$ cells 2.5 DPW in the wounds of GLPG1205-fed mice compared to vehicle-fed (methyl cellulose [MC]) control mice (Figure 1C). Total macrophage numbers were reduced by ~60% (Figure 1D), while wound-bed monocytes and neutrophils were only modestly decreased in GLPG1205-treated animals (Figures 1C and 1E). Notably, there was a ~50% reduction in unpolarized macrophages ($Ly6C^{low}$, $CD206^-$) with a ~60% reduction in $CD206^+$ macrophages (Figure S2G). These data demonstrate that GPR84 signaling supports macrophage numbers in the skin following injury.

Since macrophage numbers were not impacted in NW skin (Figure S2A), and monocyte numbers were not significantly reduced by GLPG1205 (Figure 1E), it is possible that myeloid cell chemotaxis to the site of inflammation was impacted, similar to studies in the liver.[32] Therefore, we speculated that providing a ligand for GPR84 would increase macrophage numbers in the wound. GPR84 is activated by FFAs 9–14 carbons in length, and the strongest activation is by DA.[30] Therefore, we injected DA intradermally at the periphery of the wound to determine if GPR84 activation can increase myeloid cell numbers after injury. DA was injected 24 h after injury (Figure 2A), when adipocyte lipolysis naturally contributes to MCFA levels.[27] Interestingly, 2 DPW, DA-treated wounds contained nearly double the number of $CD45^+$ cells compared to wounds from vehicle-treated animals (Figure 2B). DA treatment increased the number of total wound macrophages and $Ly6C^{hi}$ macrophages by 2-fold (Figure 2C), while $CD206^+$ macrophages increased modestly (Figure S2H). Additionally, the total number of monocytes was increased, as $Ly6C^{hi}$ monocytes and total neutrophils doubled (Figures 2D and 2E). These data support that local injection of a GPR84 agonist increases immune cell numbers after injury, promoting wound inflammation. Surprisingly, while GPR84 inhibition had little effect on pro-inflammatory macrophages, DA increased $Ly6C^{hi}$ macrophage numbers. Spatial analysis of sections immunostained for F4/80 revealed that DA injections mainly increased macrophage numbers in the wound periphery, with the most significant increases being 1.3–1.5 mm away from the wound edge (Figure 2F).

To confirm that the effect of DA on immune cell numbers was dependent on GPR84 signaling, we next treated mice with GLPG1205 or MC starting 1 day before injury and injected DA or vehicle (BSA) 1 DPW. Flow cytometry analysis revealed that in the presence of MC, DA injections still nearly doubled the $CD45^+$ population in the wounds, and this effect was abrogated by GLPG1205 administration (Figure 2G). Additionally, DA and GLPG co-treatment had no impact on wound size (Figure S2I). These findings indicate that GPR84 signaling contributes to myeloid cell infiltration of skin wounds, consistent with *in*

vitro findings that the activation of GPR84 can promote chemotaxis and pro-inflammatory activity in macrophages.[32,39,58]

Inhibition of GPR84 during the inflammation phase impairs epidermal repair

Proper regulation of the inflammatory phase is required to support efficient progression into the proliferation phase of tissue repair.[20,21,23,59] Since GLPG1205 treatment reduced macrophage numbers during the inflammation phase, we hypothesized that the inhibition of GPR84 signaling during this time would impair reparative processes during the proliferation phase of repair, similar to other studies that experimentally reduced inflammatory macrophage numbers during acute wound healing.[20,21,23,59,60] We examined epithelial repair by harvesting skin wounds 7 DPW and immunostaining sections from the center of wound beds to assess multiple cellular processes that support wound closure, including re-epithelialization (Figure 3A).[61] ITGA6 immunostaining revealed that re-epithelialization was reduced by over 25% by GLPG1205 treatment (59.54% ± 9.89%) compared to controls (98.70% ± 1.30%) (Figures 3B and 3C), with only 25% of the wounds closed in GLPG1205-treated mice compared to 80% of wounds being closed in the vehicle-fed control group (Figure 3D, $p = 0.10$). This decrease in wound closure was not associated with a change in wound width or size, suggesting that wound contraction was unaltered in response to GLPG1205 treatment during the inflammation phase (Figure 3E).[54,62,63] We next examined properties of the wound epithelium that would determine if alterations in epithelial cell migration and proliferation *in vivo* contributed to impaired wound closure. Quantification of the wound epithelium length and area revealed no change in GLPG1205-treated mice (Figures 3F and 3G), suggesting that GPR84 does not contribute to epithelial cell migratory abilities. In line with this premise, the epithelial angle of migration was steeper in GLPG1205-treated animals, indicating vertical migration into the wound as opposed to horizontal migration across the wound bed surface (Figure 3H). This altered angle of epithelial migration suggests that defects in the underlying dermal composition and function contribute to impaired wound closure. To assess epithelial cell proliferation, we quantified the number of mitotic phospho-histone $H3^+$ ($PH3^+$) cells in the wound epidermis 7 DPW. We detected no change in $PH3^+$ cells in the wound epithelium of GLPG1205-treated animals (Figures 3I and 3J), suggesting that GPR84 inhibition does not affect epithelial proliferation.[64,65] Taken together, these results indicate that early GPR84 signaling is required to support wound closure in the skin during acute wound healing.

Dermal repair is delayed by GPR84 inhibition during the inflammation phase

Our analysis of epidermal repair implicated that alterations in the dermal compartment contribute to impaired wound closure. To analyze parameters of tissue repair that would contribute to wound resolution, we assessed wound beds for fibroblast repopulation (ER-TR7), re-vascularization (CD31), and global proliferation (PH3) (Figure 4A).[22,27,66] GLPG1205 treatment reduced fibroblast infiltration to the wound by 20% (Figures 4B and 4C), while the total wound area was similar to vehicle-treated mice (Figure 4D). Since macrophage numbers are known to affect wound revascularization,[23,56,67] we quantified the area of the wound bed occupied by vascular endothelial cells through CD31 immunostaining. Interestingly, the total revascularized area was not significantly impacted at 7 DPW; however, CD31 staining was biased toward the wound edges in GLPG1205-

treated animals (Figures 4E–4H). This contrasted with a greater distribution of CD31 staining in the middle of wound beds from vehicle-treated control animals, suggesting that wound-bed revascularization was delayed in GLPG1205-fed mice. PH3 staining revealed similar numbers of dividing cells between the two conditions, suggesting that dermal cell proliferation was not significantly altered due to GPR84 inhibition (Figures 4I and 4J). Taken together, these data indicate that a GPR84-mediated reduction in infiltrating myeloid cells early during inflammation results in delayed wound repair, which in turn impacts the epithelium's ability to close the wound. Future in-depth mechanistic studies are needed to dissect whether these changes occur through direct GPR84 signaling to multiple cell types or if GPR84-dependent changes in the function of one cell type indirectly result in downstream delays in other cellular processes.

Stimulated lipolysis and MCFA abundance are reduced during early inflammation in murine diabetic skin wounds

Our results implicate GPR84 signaling as a targetable mechanism for influencing myeloid cell numbers during inflammation. Since reduced numbers of infiltrating macrophages during the early stages of repair are associated with impaired type 2 diabetic wound healing (Figures S3A–S3E),[11,16,68] we investigated if GPR84 signaling components are altered in diabetic mouse skin. Consistent with other reports, we observed a 4-fold expansion of the dermal white adipose tissue (DWAT) in obese db/db mice compared to lean db/+ controls (Figures S4A–S4C).[69] This obesity-associated expansion of the DWAT resulted from a 30% increase in adipocyte numbers (Figure S4C) and a 3-fold increase in the average cross-sectional area of dermal adipocytes (Figure S4C). With type 2 diabetes, subcutaneous and visceral white adipocytes that have a large cross-sectional area exhibit impaired stimulated lipolysis.[69–71] To explore whether injury-induced (stimulated) dermal adipocyte lipolysis was impaired in diabetic obese mice, we analyzed changes in adipocyte size in the DWAT adjacent to the wound edge (Figure 5A). Similar to our previous report, the adipocyte cross-sectional area increased early after injury, followed by a dramatic decrease between 16 h post-wounding (HPW) and 1.5 DPW in db/+ control mice (Figure 5B).[27] Interestingly, the average cross-sectional area of dermal adipocytes did not change significantly over this time period in db/db mice (Figure 5B). We further interrogated this diabetes-related reduction in lipid dynamics by examining molecular markers of stimulated lipolysis. Upon stimulation, Perilipin 1 is phosphorylated to allow enzymatic cleavage of non-esterified fatty acids (NEFAs) from stored TGs.[72–74] At 16 HPW, many dermal adipocytes at the wound edges were phospho-Perilipin 1^+ ($pPLIN1^+$) in db/+ mice but not in db/db mice (Figure 5C). To explore how impaired adipocyte lipolysis contributes to changes in local NEFAs, we performed quantitative lipid mass spectrometry with gas chromatography mass spectrometry (GC/MS) on tissue samples from uninjured skin and the wound edge of lean and diabetic mice 1 DPW. While uninjured db/db skin contains significantly more TGs than lean controls with an altered TG and NEFA composition (Figure S4D), we observed a significant reduction in the quantity of multiple NEFA species at the wound edge 1 DPW (Figure 5D). The diabetic murine wound periphery skin contained reduced quantities of the MCFAs octanoic acid (8:0) and DA (10:0). Instead, NEFAs in diabetic tissue contained greater amounts of hexadecenoic acid (16:0), and palmitoleic acid (16:1) at the wound edge

1 DPW (Figure 5D). Taken together, these data reveal a reduced presence of MCFAs in db/db wounds that could function as ligands for GPR84.

While decreased amounts of MCFAs would significantly reduce GPR84 signaling during diabetic wound healing, changes in GPR84 expression could also contribute to altered signaling. To assess diabetes-related changes in GPR84 expression during injury-induced inflammation, we compared *Gpr84* expression between different cellular subsets in NW and 1.5 DPW skin from db/db mice and db/+ lean controls. Similar to C57 mice (Figure 1A), *Gpr84* expression in db/+ and db/db NW skin is predominantly found in macrophages (Figure 5E). Strikingly, 1.5 DPW immune and stromal cells from db/db mice possessed over 2-fold greater levels of *Gpr84* than their lean controls (Figure 5F). These data suggest that diabetic skin possesses the ability to receive GPR84 signals after injury but contains reduced MCFA levels compared to lean counterparts.

DA increases myeloid cell numbers in murine diabetic skin wounds

Since diabetic mice have similar *Gpr84* expression profiles but lower ligand levels after injury, we speculated that the administration of MCFAs may rescue the reduced myeloid cell numbers during the inflammation phase in db/db mice. To test this, we intradermally injected DA or a vehicle control into db/db mice 1 DPW, when pro-inflammatory signaling is essential to recruit macrophages.[1] Wounds were harvested 2 DPW for flow cytometry analysis of myeloid cell populations and compared to db/+ mice receiving local vehicle injections (Figure 6A). In db/db mice, DA injections improved $CD45^+$ cell numbers to nearly match those of db/+ lean vehicle controls (Figure 6B). Interestingly, neutrophils increased above db/db and db/+ vehicle-injected wounds (Figure 6B), with macrophage and monocyte numbers rescued to nearly match the numbers in db/+ mice (Figures 6C and 6D). Notably, DA injection increased the number of $Ly6C^{hi}$ macrophages by 4-fold over vehicle-injected db/db wounds and increased unpolarized macrophages 3-fold (Figure 6C). While $Ly6C^{hi}$ monocytes increased modestly compared to vehicle controls, unpolarized monocyte numbers increased significantly (Figure 6D). To assess the location with increased immune cell numbers, wound beds were manually dissected from the wound periphery and analyzed using flow cytometry (Figure 6E). DA injections increased immune cells in db/+ mice at the wound periphery (Figures S5A and S5B), similar to C57 mice (Figure 2F). Interestingly, DA injections caused a significant increase in nearly all populations of immune cells in the wound bed and wound periphery; however, the increased numbers of cells in the wound beds were markedly greater than those at the wound periphery (Figures 6F–6H). Notably, total macrophages increased nearly 4-fold in db/db wound beds (Figure 6G). Though increased neutrophil infiltration is associated with poor healing in diabetic wounds,[16,75] GPR84 signaling has been shown to improve neutrophil function.[76] Thus, future lines of investigation are needed to determine how the DA-induced increase in myeloid cell numbers improves the pro-inflammatory environment necessary for proper wound resolution.

Local injection of DA during the inflammation phase improves closure and revascularization of murine diabetic wounds

To test the impact of DA-induced myeloid cell recruitment on diabetic wound healing, DA- and vehicle-injected db/db mice were allowed to heal until 7 DPW. At this point, db/db skin wounds are characteristically not fully re-epithelialized and lack proper revascularization[45,77]; however, due to the increased presence of pro-inflammatory macrophages 2 DPW (Figure 6C), we speculated that DA injection could improve tissue repair.[19] Indeed, ITGA6 staining showed an improvement in wound closure (Figures 7A–7C). Notably, ~80% of DA-treated diabetic wounds were fully closed, compared to ~33% of vehicle-treated wounds (Figure 7B), while wound width remained unchanged (Figure 7D). DA treatment also reduced $PH3^+$ cells in the wound epithelium, without impacting the area of the wound epithelium or the length of the epidermis (Figures 7E–7H). This reduction in proliferative epithelial cells is consistent with more fully closed wounds (Figure 7B). The improvement in wound closure can be attributed to the angle of migration being closer to 180° (horizontal), allowing the leading edges to merge rather than descend into the wound bed (Figure 7I), implicating improved healing in the underlying dermal compartment of DA-treated diabetic mice.

Since the wound epithelium requires a substrate to direct its migration, we speculated that the DA-treated db/db wounds may have improved dermal reconstitution. Thus, we assessed revascularization and fibroblast repopulation. Consistent with previous characterizations of db/db wounds, vehicle-treated mice had poor revascularization of the wounds based on CD31 immunostaining. DA treatment significantly increased blood vessels 7 DPW (Figures 7J–7L). Additionally, ER-TR7 and total wound area remained similar (Figures 7M–7O), while $PH3^+$ cells per mm^2 slightly decreased (Figures 7P and 7Q). This confirms that injection of DA at a single time point increases myeloid cell numbers early during diabetic wound healing and can produce a long-term improvement in skin wound healing.

DISCUSSION

The innate immune response is influenced by a plethora of factors that are concentrated at the site of injury.[78,79] We detected greater expression of *Gpr84* in multiple cell types during the inflammation phase of repair. This expression profile is in line with studies demonstrating that GPR84 levels increase in response to pro-inflammatory molecules such as IL-1β, interferon γ, lipopolysaccharide, or TNF-α.[35–37,80] *Gpr84* was detected in numerous cutaneous immune and stromal cell subsets. This suggests the potential for MCFA/GPR84 signaling to be directly received by both infiltrating myeloid cells and tissue-resident non-immune cells. While we observed *Gpr84* expression in multiple cell types in the skin (Figure 1A), consistent with findings in the kidney, adipose tissue, skeletal muscle, and stomach,[36,37,81–83] the function of GPR84 signaling in non-immune cells is not well characterized. Given that tissue-resident non-immune cells act as first responders to skin wounding, helping to initiate the pro-inflammatory cascade,[27,48,49,84–87] future studies aimed at targeting GPR84 in a cell-specific manner will further our understanding of the cellular and molecular components that coordinate injury-induced inflammation.

Fatty acids have the potential to regulate multiple facets of macrophage, B cell, dendritic cell, and T cell function.[88–93] Specifically, lipid signaling can directly regulate inflammation through various FFA receptors, including GPR120, GPR43, GPR41, and GPR40.[94–97] To date, GPR84 is the only recognized MCFA receptor with an immediate influence on innate immune cell function.[28–30,35,98] While there are contradicting reports of whether GPR84 activation induces changes in myeloid cell pro-inflammatory gene expression, GPR84 signaling directly increases macrophage phagocytic function and migration.[29,33,34,36,37,76] Interestingly, the pro-migratory nature of GPR84 signaling is conserved in *Drosophila*, mouse, and human cells.[31,33,43,76] Consistent with a role for MCFA signaling supporting myeloid cell numbers during inflammation, local injections of DA to murine skin wounds increased pro-inflammatory Ly6C^{hi} macrophage and monocyte numbers and systemic administration of the selective functional GPR84 antagonist GLPG1205 reduced macrophage numbers in wound beds. A similar reduction in myeloid cell numbers has been observed during inflammation of the liver and large intestine as a result of GPR84 inhibition.[32,39,52]

Following tissue damage, robust inflammation is required to recruit sufficient numbers of immune cells to initiate downstream reparative processes.[43,59] Specifically, a complete or partial myeloid cell depletion results in delayed revascularization and wound healing.[20,21,23,54] In line with this premise, treatment with GLPG1205 resulted in altered CD31 distribution, decreased wound closure, and reduced fibroblast infiltration at 7 DPW. Therefore, GPR84-mediated signaling during inflammation is necessary to support the subsequent proliferation phase of tissue repair. Some, but not all, clinical trials support the use of GPR84 antagonists to treat diseases associated with inflammation and fibrosis.[37,42,99,100] Since the transition to the proliferation phase requires a reduction in pro-inflammatory macrophages and the promotion of pro-healing macrophages,[23,24,54] it will be important to determine whether the timing of GPR84 manipulation during different stages of wound healing promotes tissue repair in conditions associated with chronic inflammation.

Despite higher baseline inflammation, diabetic wounds fail to mount a robust early pro-inflammatory myeloid cell response.[7,11,12,16,68] In diabetic mice and humans, adipocytes undergo higher baseline lipolysis, but stimulated lipolysis is significantly impaired.[69–71,101] Intriguingly, it was reported that GPR84 expression and activation are higher in type 2 diabetics.[50] We observed greater GPR84 expression with severely reduced levels of MCFAs in diabetic mouse skin wounds relative to lean controls. These features suggest that GPR84 activation could have therapeutic potential in diseases with reduced acute inflammatory responses. Indeed, DA injections at the wound periphery during early inflammation increased myeloid cell numbers in both C57 and db/db mice. Concordantly, DA injections improved downstream revascularization and wound closure at 7 DPW in db/db mice. While local DA injections increased neutrophil numbers, it is possible that DA reduced their detrimental effects on wound healing by enhancing neutrophil function or resolution.[18,76,102] Future lines of investigation should be aimed at determining whether the manipulation of GPR84 signaling has a similar beneficial effect in chronic wounds or diseases with impaired acute inflammatory responses in humans.

In summary, our data reveal a critical role for GPR84 signaling in promoting the pro-inflammatory myeloid response early during acute wound healing. Its manipulation has immediate effects on macrophage and monocyte numbers at the wound site, with substantial impacts downstream during the proliferation phase. Lipid signaling also contributes to the resolution of inflammation,[92,103] and the promotion of pro-healing macrophages during the transition to the proliferation phase accelerates healing.[22,23] These findings are consistent with GPR84 signaling as a component of stromal-mediated control of pro- and anti-inflammatory cues in cutaneous wounds. Further exploration of lipid signaling axes during injury-induced inflammation may lead to therapies to accelerate cutaneous wound healing or reduce cutaneous scarring associated with chronic inflammation.

Limitations of the study

These findings implicate GPR84 in propagating lipid-mediated inflammation at the wound site; however, the systemic application of GLPG1205 and the non-specific activity of DA leave questions regarding which cells are the direct mediators of GPR84 signaling. Considering that multiple cell subsets express *Gpr84* after injury, it remains likely that GPR84 signaling, and the phenotypes associated with altered GPR84 signaling, are not restricted to a singular cell type. Since this work did not utilize mouse models with a targeted genetic mutation or knockout of *Gpr84*, further lines of investigation using genetic mouse models are required to explore mechanisms that connect GPR84 signaling to the function of myeloid cells, adipocytes, and fibroblasts during wound healing. Additionally, while local administration of DA results in an increased number of myeloid cells, which is abrogated by systemic application of GLPG1205, the potential off-target effects of DA and its metabolites cannot be entirely ruled out. Lastly, the time points observed encompass acute wound healing. It will be important to continue investigations during the remodeling phase to elucidate the long-term impacts of GPR84 manipulation on scarring and extracellular matrix components that may be impacted by changes in acute inflammation.

STAR★METHODS

RESOURCE AVAILABILITY

Lead contact—Further information and requests for resources and reagents should be directed to and will be fulfilled by the lead contact, Brett Shook (brettshook@gwu.edu).

Materials availability—This study did not generate new unique reagents. Further information and requests for reagents and resources should be directed to and will be fulfilled by the lead contact.

Data and code availability

- Numerical data reported in this paper will be shared by the lead contact upon request. This paper does not report original code.
- Any additional information required to reanalyze the data reported in this paper is available from the lead contact upon request.

EXPERIMENTAL MODEL AND SUBJECT DETAILS

Wild-type C57BL/6/J (Stock #000664) and B6.BKS(D)-Lepr^{db}/J mice (Stock #000697; db/db) were purchased from The Jackson Laboratory. Animals were bred and maintained in an Association for Assessment and Accreditation of Laboratory Animal Care (AALAC)-accredited facility at the George Washington University. Male mice were used in all studies, with female mice used in key experiments to determine if major phenotypes were sex-specific. Tail vein blood was collected to determine the diabetic status of mice using a Contour Next blood glucose monitoring system. Animals were maintained in a 12-h light/dark cycling, environment with standard chow (Teklad 2018SX) provided *ad libidum*. Two to three mice were housed per cage post-wounding. All procedures were approved and in accordance with the Institutional Animal Care and Use Committee (IACUC).

METHOD DETAILS

Dorsal skin excision—8-12-week-old mice were shaved to ensure they were in the telogen phase of the hair cycle prior to wounding. Mice were anesthetized using isoflurane before 2 or 4 full-thickness excision wounds were produced by a 4 mm biopsy punch (Miltex). Animals were sacrificed at the indicated time points post-wounding, and skin samples were processed for further analysis.

GLPG1205 treatment—GLPG1205 (Galapagos Pharmaceuticals) was suspended as a slurry with constant stirring in 0.5% methyl cellulose (Sigma) dissolved in ultrapure water to a final dilution of 3 mg/mL. The slurry was administered every 12 h by oral gavage at 30 mg/kg (10 μL/g mouse), using 1.5-inch feeding needles (Fisher Scientific).

Decanoic acid treatment—Decanoic acid (DA; Sigma) was suspended in 0.5% BSA in 1X phosphate buffered saline (PBS) to a dilution of 5 mg/mL. DA suspension was warmed to 37°C for 15 min and vortexed thoroughly before use to ensure an emulsion was formed. Mice were anesthetized with isoflurane, and 20 μL of the DA solution or 0.5% BSA (Sigma, vehicle) was injected intradermally at four equidistant points around each wound on either side of the mouse.

Flow cytometry—To assess myeloid cells, wounded and uninjured skin was collected and minced by scissors into ~1 mm^2 pieces before transferring to a solution of 0.25 mg/mL Liberase in RPMI1640. All wounds from each animal were pooled together as one sample unless local injections were performed. Samples were shaken at 150 RPM at a 45° angle for 1.5 h with periodic inversions. Digestion was neutralized by the addition of 0.5M EDTA and placed on ice before trituration and straining through 70 and 40 μm strainers. Each sample was stained in 500 μL total volume with the specified antibodies: CD45 (30-F1) APC-Cy7 (1:1000, Biolegend 103116), CD11b (M1/70) Alexa Fluor 700 (1:500, Biolegend 101222), F4/80 (BM8) e450 (1:100, eBioscience 48-4801-82), CD206 (C068C2) BV650 or PE-Cy5 (1:500, Biolegend 141723 or 1:1000, 141740), Ly6C (HK1.4) BV570 (1:500, Biolegend 128030), and Ly6G (1A8) BV785 or PE-Cy7 (1:500, Biolegend 127645 or 1:1000, 127618). SYTOX green (FITC; Invitrogen S34860) or Zombie Aqua (Biolegend 423102) was used as a live/dead stain per the manufacturer's protocols. Samples were analyzed on a BD FACS Celesta at the GWU flow cytometry core facility or Beckman CytoFLEX S.

Cell isolation—To isolate myeloid cells and fibroblasts, tissues were digested as described above for analysis. Each sample was then stained in 500 μL total volume with the following antibodies: CD31 (390) APC-Fire 750 (1:500, Biolegend 102434), EpCAM (G8.8) APC-Fire 750 (1:500, Biolegend 118230), CD45 (30-F11) FITC (1:1000, Biolegend 103108), CD11b (M1/70) Alexa Fluor 700 (1:500, Biolegend 101222), Ly6G (1A8) PE-Cy7 (1:1000, Biolegend 127618), F4/80 (BM8) e450 (1:200, eBioscience 48-4801-82), SYTOX orange (Invitrogen S34861) was used as a live/dead stain.

Epithelial cells, DWAT, and SVF were isolated concurrently. Fascia and DWAT were scraped from wounded and uninjured skin to expose the dermis and epidermis to digestion in 0.25% Trypsin-EDTA for 1 h at 37°C. Epithelium was then scraped from the surface, triturated, and strained through 70 and 40 μm strainers before staining with: CD45 (30-F1) APC-Cy7 (1:1000, Biolegend 103116), EpCAM/CD326 (G8.8) APC (1:100, Biolegend 118214), CD49f (ITGA6, GoH3) BV650 (1:500, BD Biosciences 563707), and SYTOX green. Concurrently, the scraped fascia and DWAT was digested as described above. After centrifugation, both the floating dermal adipocytes and pelleted stromal vascular fraction (SVF) were immediately lysed in TRIzol. Sorted samples were obtained on a BD Influx at the GWU flow cytometry core facility.

Immunofluorescence and imaging—Mouse skin and wounds were embedded in Optimal Cutting Temperature (O.C.T.; Sakura) and quickly frozen on dry ice. Wounds were sectioned in their entirety at 16 μm thickness to identify sections at the center of the wound bed.[104] Oblong or oval-shaped wounds were not included in our analysis, as the kinetics of assessing tissue repair from the central sections of the wounds will differ from the expected circular-shaped wounds. Tissue was briefly fixed in 4% formaldehyde and blocked in 10% normal donkey serum (NDS) before staining with the following primary antibodies at 4°C overnight: CD31 (1:50, BD Pharmigen 550274), CD68 (1:500, Abcam ab155212), ER-TR7 (1:500, Abcam ab51824), F4/80 (1:200, Abcam ab6640), Integrin alpha6 (1:500, R&D Systems MAB 13501), Keratin17 (1:1000, Biolegend 697202), Perilipin 1 (1:500, Abcam ab61682), phospho-Perilipin 1 (1:100, Vala Sciences 4855), phospho-Histone H3 (1:500, Abcam ab5176). Alexa Fluor conjugated secondary antibodies were applied for 1 h at 1:500 concentration. All slides were counterstained with DAPI in ProLong Gold Antifade reagent (Invitrogen). For DWAT analysis, tissues were fixed in 4% paraformaldehyde in PBS followed by 30% sucrose before embedding in O.C.T. Wound centers were identified by microscopy, and the two most central sections per slide were imaged. Two wound beds were analyzed from each mouse. Tissue sections were imaged as single fields of view or tilescans using a Zeiss AxioImager M2 with ApoTome equipped with an Orca-Flash4.0 LT Plus camera (Hamamatsu, C11440). Images were acquired using a 10× Zeiss EC Plan NEOFLUAR objective (0.3 numerical aperture) at a 0.65μm/pixel scale or 20× Zeiss Plan-APOCHROMAT objective (0.8 numerical aperture) at a 0.325μm/pixel scale. Identical parameters (objective, exposure time, and brightness and contrast adjustments) were utilized for all images compared during image analysis.

Image analysis—Quantification of key parameters was performed on the 2 most central sections of the wound, and wound results were averaged per mouse as previously

described.[22,27,66] To quantify re-epithelialization (the percentage of the wound covered by ITGA6), area of wound epithelium, and adipocyte size (PLIN1), ImageJ was used to delineate and measure the regions of interest as previously described.[61,105] The angle tool in ImageJ was used to measure the angle of epithelial migration on ITGA6 immunostained tissue sections, by setting the baseline on the epithelium adjacent to the wound edge and extending the second line halfway through the migrating tongue of epithelium.[61] To examine revascularization and fibroblast repopulation, the $CD31^+$ or $ER\text{-}TR7^+$ pixels were identified using Color Range selection in Adobe Photoshop. Identical Color Range criteria were utilized for all samples in each experiment to determine the number of $CD31^+$ or $ER\text{-}TR7^+$ pixels, which was divided by the total number of pixels per wound bed. To plot the spatial distribution of CD31, the wound bed was cropped images were normalized to 500 pixels wide, then ImageJ (FIJI 2) was used to determine the average pixel intensity for each vertical line of pixels. To determine the spatial location of macrophages in tissue sections, images were adjusted in Photoshop to remove background fluorescence using the levels tool. All images were adjusted with the same values to avoid bias. Regions of interest were outlined, and the remainder was filled black. Wound edges were cropped to a width of 1.5mm from the wound edge. Automated quantification of $F4/80^+$ cells in the wound center and periphery was performed in MATLAB R2023b. Images were divided into 100 μm bins along the horizontal axis. The vertical axes were normalized to 4000 pixels and divided into 15 bins. The nuclear and F4/80 signals were first made into binary images, and the “regionprops” command was used to identify areas of nuclear or F4/80 staining. These objects were counted as $F4/80^+$ cells if there was at least 75% overlap of the nuclear and F4/80 stains. The script reported the total number of $F4/80^+$ cells in each image as well as the number in each bin, which were used for subsequent spatial analysis along the superficial-deep and proximal-distal axes at the wound periphery.

Lipidomic analysis—Flash-frozen skin punches were pulverized, and 10 mg of the frozen pulverized tissue was used for Folch extraction. The total lipid extract was then spotted and run on a 1D-TLC for the separation of phospholipids, triglycerides, and free fatty acids (FFAs). The TLC regions containing phospholipids and triglycerides were saponified and converted into Fatty Acid Methyl Esters that were then run on a GC/MS for analysis. The FFA region from the TLC plates was extracted with 100 μL 1:1 chloroform:methanol, and the silicon solid phase was pelleted at 12,000 x g for 3 min. The FFA extracts were mixed with 20 ng blended stable isotope internal standard, taken to dryness under gaseous N_2, and resuspended in 25 μL of 1% pentafluorobenzyl bromide in acetonitrile to which 25 μL of 1% diisopropylethylamine in acetonitrile was added, and samples were derivatized at room temperature for 30 min. Pentafluorbenzyl-fatty acid derivatives were taken to dryness under gaseous N_2 and resuspended in 80 μL hexanes. 1 μL of pentafluorbenzyl-fatty acid derivatives was injected and data were collected by GC-MS running in NCI mode (8890 GC, 5977B MSD, Agilent) using the DB-FatWax column (G3903-63008, Agilent) with the following run program: injector temp was 250°C, 80°C hold for 1 min, 30 °C/min ramp to 125°C, no hold, 50°C ramp to 250°C and hold for 20 min. The flow for the methane carrier gas was set at 1.5 mL/min.

Cell culture and pharmacologic agents—Bone marrow-derived macrophages (BMDMs) were obtained from the femur and tibia of adult wild-type mice. After ACK lysis, cells were seeded at 4×10^6 into 10 cm petri dishes and cultured at 37°C and 5% CO_2 in RPMI with 10% FBS, 1% antibiotic-antimycotic, and 30% L929 conditioned media, with replenishment 4 days post-plating. After 7 days, cells were passaged the day before stimulation. 10,000 cells were seeded per well of a 96-well plate in 100 μL of serum-free RPMI with 1% antibiotic-antimycotic. The BMDMs were stimulated with 10 ng/mL of LPS for 2 h before the addition of GPR84 agonists or antagonists suspended in DMSO. Cells were treated with 50 μM of GLPG1205 for 30 min before the addition of 500 nM 6-OAU or 25 μM DA for 2 h prior to harvesting.

RNA isolation and quantitative real-time PCR—Samples were digested in TRIzol (Invitrogen), and RNA was purified by phase separation followed by the use of the RNeasy Plus Micro Kit (Qiagen). cDNA was produced from the purified RNA using Invitrogen's Superscript IV First-Strand Synthesis Kit. Gene targets were assessed with SYBR PowerTrack Green master mix (Applied Biosystems) and gene-specific primers (IDT) using a CFX384 detection system with a C1000 thermocycler (Bio-Rad). Results were normalized to corresponding *Actnb* and fold changes in gene expression were generated based on specified cell populations.

STATISTICS

To determine the significance between two groups, a comparison was made using the two-tailed Student's t-test. To compare the percentage of open versus closed wounds a Fisher's exact test was used. Analyses across multiple groups were made using a one-way analysis of variance (ANOVA) with Bonferroni's post hoc test, one-way ANOVA corrected for multiple comparisons using two-stage setup method of Benjamini, Krieger, and Yekutieli, Brown-Forsythe and Welch ANOVA test or a two-way ANOVA with Šidák correction using GraphPad Prism for Mac (GraphPad Software, La Jolla, CA) with significance set at $p < 0.05$.

Supplementary Material

Refer to Web version on PubMed Central for supplementary material.

ACKNOWLEDGMENTS

This work is supported in part by an NIH grant to B.A.S. from NIAMS (AR082417) and a start-up fund from The George Washington University (GWU) to B.A.S. M.C.R. is supported by DK122189-01 and DK109079. P.O.C. is supported by a training grant through The GWU Cancer Center (T32 CA247756). We thank Galapagos NV for providing GLPG1205 and Dr. Laurent Sanière for technical assistance related to GLPG1205 usage. We thank members of the Shook Lab for their assistance in processing samples and critical reading of the manuscript.

REFERENCES

1. Eming SA, Krieg T, and Davidson JM (2007). Inflammation in wound repair: molecular and cellular mechanisms. J. Invest. Dermatol. 127, 514–525. 10.1038/sj.jid.5700701. [PubMed: 17299434]
2. Ridiandries A, Tan JTM, and Bursill CA (2018). The Role of Chemokines in Wound Healing. Int. J. Mol. Sci. 19, 3217. 10.3390/ijms19103217. [PubMed: 30340330]

3. de Oliveira S, Rosowski EE, and Huttenlocher A (2016). Neutrophil migration in infection and wound repair: going forward in reverse. Nat. Rev. Immunol. 16, 378–391. 10.1038/nri.2016.49. [PubMed: 27231052]

4. Gurtner GC, Werner S, Barrandon Y, and Longaker MT (2008). Wound repair and regeneration. Nature 453, 314–321. 10.1038/nature07039. [PubMed: 18480812]

5. Zomer HD, and Trentin AG (2018). Skin wound healing in humans and mice: Challenges in translational research. J. Dermatol. Sci. 90, 3–12. 10.1016/j.jdermsci.2017.12.009. [PubMed: 29289417]

6. Eming SA, Martin P, and Tomic-Canic M (2014). Wound repair and regeneration: mechanisms, signaling, and translation. Sci. Transl. Med. 6, 265sr6. 10.1126/scitranslmed.3009337. [PubMed: 25473038]

7. Nassiri S, Zakeri I, Weingarten MS, and Spiller KL (2015). Relative Expression of Proinflammatory and Antiinflammatory Genes Reveals Differences between Healing and Nonhealing Human Chronic Diabetic Foot Ulcers. J. Invest. Dermatol. 135, 1700–1703. 10.1038/jid.2015.30. [PubMed: 25647438]

8. Davis FM, Tsoi LC, Wasikowski R, denDekker A, Joshi A, Wilke C, Deng H, Wolf S, Obi A, Huang S, et al. (2020). Epigenetic regulation of the PGE2 pathway modulates macrophage phenotype in normal and pathologic wound repair. JCI Insight 5, e138443. 10.1172/jci.insight.138443. [PubMed: 32879137]

9. Boniakowski AE, Kimball AS, Jacobs BN, Kunkel SL, and Gallagher KA (2017). Macrophage-Mediated Inflammation in Normal and Diabetic Wound Healing. J. Immunol. 199, 17–24. 10.4049/jimmunol.1700223. [PubMed: 28630109]

10. Mirza RE, Fang MM, Weinheimer-Haus EM, Ennis WJ, and Koh TJ (2014). Sustained inflammasome activity in macrophages impairs wound healing in type 2 diabetic humans and mice. Diabetes 63, 1103–1114. 10.2337/db13-0927. [PubMed: 24194505]

11. Mirza R, and Koh TJ (2011). Dysregulation of monocyte/macrophage phenotype in wounds of diabetic mice. Cytokine 56, 256–264. 10.1016/j.cyto.2011.06.016. [PubMed: 21803601]

12. Louiselle AE, Niemiec SM, Zgheib C, and Liechty KW (2021). Macrophage polarization and diabetic wound healing. Transl. Res. 236, 109–116. 10.1016/j.trsl.2021.05.006. [PubMed: 34089902]

13. Gould L, Abadir P, Brem H, Carter M, Conner-Kerr T, Davidson J, DiPietro L, Falanga V, Fife C, Gardner S, et al. (2015). Chronic wound repair and healing in older adults: current status and future research. J. Am. Geriatr. Soc. 63, 427–438. 10.1111/jgs.13332. [PubMed: 25753048]

14. Audu CO, Melvin WJ, Joshi AD, Wolf SJ, Moon JY, Davis FM, Barrett EC, Mangum KD, Deng H, Xing X, et al. (2022). Macrophage-specific inhibition of the histone demethylase JMJD3 decreases STING and pathologic inflammation in diabetic wound repair. Cell. Mol. Immunol. 19, 1251–1262. 10.1038/s41423-022-00919-5. [PubMed: 36127466]

15. Vu R, Jin S, Sun P, Haensel D, Nguyen QH, Dragan M, Kessenbrock K, Nie Q, and Dai X (2022). Wound healing in aged skin exhibits systems-level alterations in cellular composition and cell-cell communication. Cell Rep. 40, 111155. 10.1016/j.celrep.2022.111155. [PubMed: 35926463]

16. Joshi N, Pohlmeier L, Ben-Yehuda Greenwald M, Haertel E, Hiebert P, Kopf M, and Werner S (2020). Comprehensive characterization of myeloid cells during wound healing in healthy and healing-impaired diabetic mice. Eur. J. Immunol. 50, 1335–1349. 10.1002/eji.201948438. [PubMed: 32306381]

17. DiPietro LA, Burdick M, Low QE, Kunkel SL, and Strieter RM (1998). MIP-1alpha as a critical macrophage chemoattractant in murine wound repair. J. Clin. Invest. 101, 1693–1698. 10.1172/JCI1020. [PubMed: 9541500]

18. Sawaya AP, Stone RC, Brooks SR, Pastar I, Jozic I, Hasneen K, O'Neill K, Mehdizadeh S, Head CR, Strbo N, et al. (2020). Deregulated immune cell recruitment orchestrated by FOXM1 impairs human diabetic wound healing. Nat. Commun. 11, 4678. 10.1038/s41467-020-18276-0. [PubMed: 32938916]

19. Wood S, Jayaraman V, Huelsmann EJ, Bonish B, Burgad D, Sivaramakrishnan G, Qin S, DiPietro LA, Zloza A, Zhang C, and Shafikhani SH (2014). Pro-inflammatory chemokine CCL2 (MCP-1)

promotes healing in diabetic wounds by restoring the macrophage response. PLoS One 9, e91574. 10.1371/journal.pone.0091574. [PubMed: 24618995]

20. Goren I, Allmann N, Yogev N, Schürmann C, Linke A, Holdener M, Waisman A, Pfeilschifter J, and Frank S (2009). A transgenic mouse model of inducible macrophage depletion: effects of diphtheria toxin-driven lysozyme M-specific cell lineage ablation on wound inflammatory, angiogenic, and contractive processes. Am. J. Pathol. 175, 132–147. 10.2353/ajpath.2009.081002. [PubMed: 19528348]
21. Mirza R, DiPietro LA, and Koh TJ (2009). Selective and specific macrophage ablation is detrimental to wound healing in mice. Am. J. Pathol. 175, 2454–2462. 10.2353/ajpath.2009.090248. [PubMed: 19850888]
22. Shook BA, Wasko RR, Rivera-Gonzalez GC, Salazar-Gatzimas E, López-Giráldez F, Dash BC, Muñoz-Rojas AR, Aultman KD, Zwick RK, Lei V, et al. (2018). Myofibroblast proliferation and heterogeneity are supported by macrophages during skin repair. Science 362, eaar2971. 10.1126/science.aar2971. [PubMed: 30467144]
23. Shook B, Xiao E, Kumamoto Y, Iwasaki A, and Horsley V (2016). CD301b+ Macrophages Are Essential for Effective Skin Wound Healing. J. Invest. Dermatol. 136, 1885–1891. 10.1016/j.jid.2016.05.107. [PubMed: 27287183]
24. Pang J, Maienschein-Cline M, and Koh TJ (2022). Monocyte/Macrophage Heterogeneity during Skin Wound Healing in Mice. J. Immunol. 209, 1999–2011. 10.4049/jimmunol.2200365. [PubMed: 36426946]
25. Aitcheson SM, Frentiu FD, Hurn SE, Edwards K, and Murray RZ (2021). Skin Wound Healing: Normal Macrophage Function and Macrophage Dysfunction in Diabetic Wounds. Molecules 26, 4917. 10.3390/molecules26164917. [PubMed: 34443506]
26. Bannon P, Wood S, Restivo T, Campbell L, Hardman MJ, and Mace KA (2013). Diabetes induces stable intrinsic changes to myeloid cells that contribute to chronic inflammation during wound healing in mice. Dis. Model. Mech. 6, 1434–1447. 10.1242/dmm.012237. [PubMed: 24057002]
27. Shook BA, Wasko RR, Mano O, Rutenberg-Schoenberg M, Rudolph MC, Zirak B, Rivera-Gonzalez GC, López-Giráldez F, Zarini S, Rezza A, et al. (2020). Dermal Adipocyte Lipolysis and Myofibroblast Conversion Are Required for Efficient Skin Repair. Cell Stem Cell 26, 880–895.e6. 10.1016/j.stem.2020.03.013. [PubMed: 32302523]
28. Mahmud ZA, Jenkins L, Ulven T, Labéguère F, Gosmini R, De Vos S, Hudson BD, Tikhonova IG, and Milligan G (2017). Three classes of ligands each bind to distinct sites on the orphan G protein-coupled receptor GPR84. Sci. Rep. 7, 17953. 10.1038/s41598-017-18159-3. [PubMed: 29263400]
29. Suzuki M, Takaishi S, Nagasaki M, Onozawa Y, Iino I, Maeda H, Komai T, and Oda T (2013). Medium-chain fatty acid-sensing receptor, GPR84, is a proinflammatory receptor. J. Biol. Chem. 288, 10684–10691. 10.1074/jbc.M112.420042. [PubMed: 23449982]
30. Wang J, Wu X, Simonavicius N, Tian H, and Ling L (2006). Medium-chain fatty acids as ligands for orphan G protein-coupled receptor GPR84. J. Biol. Chem. 281, 34457–34464. 10.1074/jbc.M608019200. [PubMed: 16966319]
31. Schulze AS, Kleinau G, Krakowsky R, Rochmann D, Das R, Worth CL, Krumbholz P, Scheerer P, and Stäubert C (2022). Evolutionary analyses reveal immune cell receptor GPR84 as a conserved receptor for bacteria-derived molecules. iScience 25, 105087. 10.1016/j.isci.2022.105087. [PubMed: 36164652]
32. Puengel T, De Vos S, Hundertmark J, Kohlhepp M, Guldiken N, Pujuguet P, Auberval M, Marsais F, Shoji KF, Saniere L, et al. (2020). The Medium-Chain Fatty Acid Receptor GPR84 Mediates Myeloid Cell Infiltration Promoting Steatohepatitis and Fibrosis. J. Clin. Med. 9, 1140. 10.3390/jcm9041140. [PubMed: 32316235]
33. Nicol LSC, Dawes JM, La Russa F, Didangelos A, Clark AK, Gentry C, Grist J, Davies JB, Malcangio M, and McMahon SB (2015). The role of G-protein receptor 84 in experimental neuropathic pain. J. Neurosci. 35, 8959–8969. 10.1523/JNEUROSCI.3558-14.2015. [PubMed: 26063927]
34. Wei L, Tokizane K, Konishi H, Yu HR, and Kiyama H (2017). Agonists for G-protein-coupled receptor 84 (GPR84) alter cellular morphology and motility but do not induce pro-inflammatory

responses in microglia. J. Neuroinflammation 14, 198. 10.1186/s12974-017-0970-y. [PubMed: 28974234]

35. Chen LH, Zhang Q, Xie X, and Nan FJ (2020). Modulation of the G-Protein-Coupled Receptor 84 (GPR84) by Agonists and Antagonists. J. Med. Chem. 63, 15399–15409. 10.1021/acs.jmedchem.0c01378. [PubMed: 33267584]
36. Recio C, Lucy D, Purvis GSD, Iveson P, Zeboudj L, Iqbal AJ, Lin D, O'Callaghan C, Davison L, Griesbach E, et al. (2018). Activation of the Immune-Metabolic Receptor GPR84 Enhances Inflammation and Phagocytosis in Macrophages. Front. Immunol. 9, 1419. 10.3389/fimmu.2018.01419. [PubMed: 29973940]
37. Gagnon L, Leduc M, Thibodeau JF, Zhang MZ, Grouix B, Sarra-Bournet F, Gagnon W, Hince K, Tremblay M, Geerts L, et al. (2018). A Newly Discovered Antifibrotic Pathway Regulated by Two Fatty Acid Receptors: GPR40 and GPR84. Am. J. Pathol. 188, 1132–1148. 10.1016/j.ajpath.2018.01.009. [PubMed: 29454750]
38. Simard JC, Thibodeau JF, Leduc M, Tremblay M, Laverdure A, Sarra-Bournet F, Gagnon W, Ouboudinar J, Gervais L, Felton A, et al. (2020). Fatty acid mimetic PBI-4547 restores metabolic homeostasis via GPR84 in mice with non-alcoholic fatty liver disease. Sci. Rep. 10, 12778. 10.1038/s41598-020-69675-8. [PubMed: 32728158]
39. Zhang Q, Chen LH, Yang H, Fang YC, Wang SW, Wang M, Yuan QT, Wu W, Zhang YM, Liu ZJ, et al. (2022). GPR84 signaling promotes intestinal mucosal inflammation via enhancing NLRP3 inflammasome activation in macrophages. Acta Pharmacol. Sin. 43, 2042–2054. 10.1038/s41401-021-00825-y. [PubMed: 34912006]
40. Yin C, Cheng L, Pan J, Chen L, Xue Q, Qin J, Wang S, Du B, Liu M, Zhang Y, et al. (2020). Regulatory role of Gpr84 in the switch of alveolar macrophages from CD11b. Mucosal Immunol. 13, 892–907. 10.1038/s41385-020-0321-7. [PubMed: 32719411]
41. Abdel-Aziz H, Schneider M, Neuhuber W, Meguid Kassem A, Khailah S, Müller J, Gamal Eldeen H, Khairy A, T Khayyal M, Shcherbakova A, et al. (2016). GPR84 and TREM-1 Signaling Contribute to the Pathogenesis of Reflux Esophagitis. Mol. Med. 21, 1011–1024. 10.2119/molmed.2015.00098. [PubMed: 26650186]
42. Vermeire S, Reinisch W, Wasko-Czopnik D, Van Kaem T, Desrivot J, Vanhoutte F, and Beetens J (2017). P610 Efficacy and safety of GLPG1205, a GPR84 antagonist, in ulcerative colitis: multi-centre proof-of-concept study. Journal of Crohn's and Colitis 11, S390–S391. 10.1093/ecco-jcc/jjx002.734.
43. Thuma L, Carter D, Weavers H, and Martin P (2018). immune cells extravasate from vessels to wounds using Tre1 GPCR and Rho signaling. J. Cell Biol. 217, 3045–3056. 10.1083/jcb.201801013. [PubMed: 29941473]
44. Labéguère F, Dupont S, Alvey L, Soulas F, Newsome G, Tirera A, Quenehen V, Mai TTT, Deprez P, Blanqué R, et al. (2020). Discovery of 9-Cyclopropylethynyl-2-((S)-1-[1,4]dioxan-2-ylmethoxy)-6,7-dihydropyrimido[6,1- a]isoquinolin-4-one (GLPG1205), a Unique GPR84 Negative Allosteric Modulator Undergoing Evaluation in a Phase II Clinical Trial. J. Med. Chem. 63, 13526–13545. 10.1021/acs.jmedchem.0c00272. [PubMed: 32902984]
45. Senter LH, Legrand EK, Laemmerhirt KE, and Kiorpes TC (1995). Assessment of full-thickness wounds in the genetically diabetic mouse for suitability as a wound healing model. Wound Repair Regen. 3, 351–358. 10.1046/j.1524-475X.1995.30316.x. [PubMed: 17173562]
46. Michaels J, Churgin SS, Blechman KM, Greives MR, Aarabi S, Galiano RD, and Gurtner GC (2007). db/db mice exhibit severe wound-healing impairments compared with other murine diabetic strains in a silicone-splinted excisional wound model. Wound Repair Regen. 15, 665–670. 10.1111/j.1524-475X.2007.00273.x. [PubMed: 17971012]
47. Lattin JE, Schroder K, Su AI, Walker JR, Zhang J, Wiltshire T, Saijo K, Glass CK, Hume DA, Kellie S, and Sweet MJ (2008). Expression analysis of G Protein-Coupled Receptors in mouse macrophages. Immunome Res. 4, 5. 10.1186/1745-7580-4-5. [PubMed: 18442421]
48. Roupé KM, Nybo M, Sjöbring U, Alberius P, Schmidtchen A, and Sørensen OE (2010). Injury is a major inducer of epidermal innate immune responses during wound healing. J. Invest. Dermatol. 130, 1167–1177. 10.1038/jid.2009.284. [PubMed: 19727116]

49. Guenin-Mace L, Konieczny P, and Naik S (2023). Immune-Epithelial Cross Talk in Regeneration and Repair. Annu. Rev. Immunol. 41, 207–228. 10.1146/annurev-immunol-101721-062818. [PubMed: 36696569]
50. Mikkelsen RB, Arora T, Trošt K, Dmytriyeva O, Jensen SK, Meijnikman AS, Olofsson LE, Lappa D, Aydin Ö, Nielsen J, et al. (2022). Type 2 diabetes is associated with increased circulating levels of 3-hydroxydecanoate activating GPR84 and neutrophil migration. iScience 25, 105683. 10.1016/j.isci.2022.105683. [PubMed: 36561890]
51. Wang SW, Zhang Q, Lu D, Fang YC, Yan XC, Chen J, Xia ZK, Yuan QT, Chen LH, Zhang YM, et al. (2023). GPR84 regulates pulmonary inflammation by modulating neutrophil functions. Acta Pharmacol. Sin. 44, 1665–1675. 10.1038/s41401-023-01080-z. [PubMed: 37016043]
52. Labéguère F, Dupont S, Alvey L, Soulas F, Newsome G, Tirera A, Quenehen V, Mai TTT, Deprez P, Blanqué R, et al. (2020). Discovery of 9-Cyclopropylethynyl-2-. J. Med. Chem. 63, 13526–13545. 10.1021/acs.jmedchem.0c00272. [PubMed: 32902984]
53. Rodero MP, Hodgson SS, Hollier B, Combadiere C, and Khosrotehrani K (2013). Reduced Il17a expression distinguishes a Ly6c(lo) MHCII(hi) macrophage population promoting wound healing. J. Invest. Dermatol. 133, 783–792. 10.1038/jid.2012.368. [PubMed: 23235530]
54. Lucas T, Waisman A, Ranjan R, Roes J, Krieg T, Müller W, Roers A, and Eming SA (2010). Differential roles of macrophages in diverse phases of skin repair. J. Immunol. 184, 3964–3977. 10.4049/jimmunol.0903356. [PubMed: 20176743]
55. Brancato SK, and Albina JE (2011). Wound macrophages as key regulators of repair: origin, phenotype, and function. Am. J. Pathol. 178, 19–25. 10.1016/j.ajpath.2010.08.003. [PubMed: 21224038]
56. Ferrante CJ, and Leibovich SJ (2012). Regulation of Macrophage Polarization and Wound Healing. Adv. Wound Care 1, 10–16. 10.1089/wound.2011.0307.
57. Daley JM, Brancato SK, Thomay AA, Reichner JS, and Albina JE (2010). The phenotype of murine wound macrophages. J. Leukoc. Biol. 87, 59–67. 10.1189/jlb.0409236. [PubMed: 20052800]
58. Gaidarov I, Anthony T, Gatlin J, Chen X, Mills D, Solomon M, Han S, Semple G, and Unett DJ (2018). Embelin and its derivatives unravel the signaling, proinflammatory and antiatherogenic properties of GPR84 receptor. Pharmacol. Res. 131, 185–198. 10.1016/j.phrs.2018.02.021. [PubMed: 29471103]
59. Konieczny P, Xing Y, Sidhu I, Subudhi I, Mansfield KP, Hsieh B, Biancur DE, Larsen SB, Cammer M, Li D, et al. (2022). Interleukin-17 governs hypoxic adaptation of injured epithelium. Science 377, eabg9302. 10.1126/science.abg9302. [PubMed: 35709248]
60. Willenborg S, Lucas T, van Loo G, Knipper JA, Krieg T, Haase I, Brachvogel B, Hammerschmidt M, Nagy A, Ferrara N, et al. (2012). CCR2 recruits an inflammatory macrophage subpopulation critical for angiogenesis in tissue repair. Blood 120, 613–625. 10.1182/blood-2012-01-403386. [PubMed: 22577176]
61. Yan S, Ripamonti R, Kawabe H, Ben-Yehuda Greenwald M, and Werner S (2022). NEDD4-1 Is a Key Regulator of Epidermal Homeostasis and Wound Repair. J. Invest. Dermatol. 142, 1703–1713.e11. 10.1016/j.jid.2021.09.033. [PubMed: 34756879]
62. Chen L, Mirza R, Kwon Y, DiPietro LA, and Koh TJ (2015). The murine excisional wound model: Contraction revisited. Wound Repair Regen. 23, 874–877. 10.1111/wrr.12338. [PubMed: 26136050]
63. Parfejevs V, Debbache J, Shakhova O, Schaefer SM, Glausch M, Wegner M, Suter U, Riekstina U, Werner S, and Sommer L (2018). Injury-activated glial cells promote wound healing of the adult skin in mice. Nat. Commun. 9, 236. 10.1038/s41467-017-01488-2. [PubMed: 29339718]
64. Park S, Gonzalez DG, Guirao B, Boucher JD, Cockburn K, Marsh ED, Mesa KR, Brown S, Rompolas P, Haberman AM, et al. (2017). Tissue-scale coordination of cellular behaviour promotes epidermal wound repair in live mice. Nat. Cell Biol. 19, 155–163. 10.1038/ncb3472. [PubMed: 28248302]
65. Aragona M, Dekoninck S, Rulands S, Lenglez S, Mascré G, Simons BD, and Blanpain C (2017). Defining stem cell dynamics and migration during wound healing in mouse skin epidermis. Nat. Commun. 8, 14684. 10.1038/ncomms14684. [PubMed: 28248284]

66. Schmidt BA, and Horsley V (2013). Intradermal adipocytes mediate fibroblast recruitment during skin wound healing. Development 140, 1517–1527. 10.1242/dev.087593. [PubMed: 23482487]

67. Leibovich SJ, and Ross R (1975). The role of the macrophage in wound repair. A study with hydrocortisone and antimacrophage serum. Am. J. Pathol. 78, 71–100. [PubMed: 1109560]

68. Lecube A, Pachón G, Petriz J, Hernández C, and Simó R (2011). Phagocytic activity is impaired in type 2 diabetes mellitus and increases after metabolic improvement. PLoS One 6, e23366. 10.1371/journal.pone.0023366. [PubMed: 21876749]

69. Verboven K, Wouters K, Gaens K, Hansen D, Bijnen M, Wetzels S, Stehouwer CD, Goossens GH, Schalkwijk CG, Blaak EE, and Jocken JW (2018). Abdominal subcutaneous and visceral adipocyte size, lipolysis and inflammation relate to insulin resistance in male obese humans. Sci. Rep. 8, 4677. 10.1038/s41598-018-22962-x. [PubMed: 29549282]

70. Jocken JWE, Langin D, Smit E, Saris WHM, Valle C, Hul GB, Holm C, Arner P, and Blaak EE (2007). Adipose triglyceride lipase and hormone-sensitive lipase protein expression is decreased in the obese insulin-resistant state. J. Clin. Endocrinol. Metab. 92, 2292–2299. 10.1210/jc.2006-1318. [PubMed: 17356053]

71. Czech MP (1976). Cellular basis of insulin insensitivity in large rat adipocytes. J. Clin. Invest. 57, 1523–1532. 10.1172/JCI108422. [PubMed: 932192]

72. Sztalryd C, and Brasaemle DL (2017). The perilipin family of lipid droplet proteins: Gatekeepers of intracellular lipolysis. Biochim. Biophys. Acta. Mol. Cell Biol. Lipids 1862, 1221–1232. 10.1016/j.bbalip.2017.07.009. [PubMed: 28754637]

73. Greenberg AS, Egan JJ, Wek SA, Garty NB, Blanchette-Mackie EJ, and Londos C (1991). Perilipin, a major hormonally regulated adipocyte-specific phosphoprotein associated with the periphery of lipid storage droplets. J. Biol. Chem. 266, 11341–11346. [PubMed: 2040638]

74. Choi SM, Tucker DF, Gross DN, Easton RM, DiPilato LM, Dean AS, Monks BR, and Birnbaum MJ (2010). Insulin regulates adipocyte lipolysis via an Akt-independent signaling pathway. Mol. Cell Biol. 30, 5009–5020. 10.1128/MCB.00797-10. [PubMed: 20733001]

75. Nguyen KT, Seth AK, Hong SJ, Geringer MR, Xie P, Leung KP, Mustoe TA, and Galiano RD (2013). Deficient cytokine expression and neutrophil oxidative burst contribute to impaired cutaneous wound healing in diabetic, biofilm-containing chronic wounds. Wound Repair Regen. 21, 833–841. 10.1111/wrr.12109. [PubMed: 24118295]

76. Sundqvist M, Christenson K, Holdfeldt A, Gabl M, Mårtensson J, Björkman L, Dieckmann R, Dahlgren C, and Forsman H (2018). Similarities and differences between the responses induced in human phagocytes through activation of the medium chain fatty acid receptor GPR84 and the short chain fatty acid receptor FFA2R. Biochim. Biophys. Acta. Mol. Cell Res. 1865, 695–708. 10.1016/j.bbamcr.2018.02.008. [PubMed: 29477577]

77. Zhao G, Hochwalt PC, Usui ML, Underwood RA, Singh PK, James GA, Stewart PS, Fleckman P, and Olerud JE (2010). Delayed wound healing in diabetic (db/db) mice with Pseudomonas aeruginosa biofilm challenge: a model for the study of chronic wounds. Wound Repair Regen. 18, 467–477. 10.1111/j.1524-475X.2010.00608.x. [PubMed: 20731798]

78. Li D, Peng H, Qu L, Sommar P, Wang A, Chu T, Li X, Bi X, Liu Q, Gallais Sérézal I, et al. (2021). miR-19a/b and miR-20a Promote Wound Healing by Regulating the Inflammatory Response of Keratinocytes. J. Invest. Dermatol. 141, 659–671. 10.1016/j.jid.2020.06.037. [PubMed: 32949564]

79. Currie HN, Loos MS, Vrana JA, Dragan K, and Boyd JW (2014). Spatial cytokine distribution following traumatic injury. Cytokine 66, 112–118. 10.1016/j.cyto.2014.01.001. [PubMed: 24461742]

80. Muredda L, Kępczyńska MA, Zaibi MS, Alomar SY, and Trayhurn P (2018). IL-1β and TNFα inhibit GPR120 (FFAR4) and stimulate GPR84 (EX33) and GPR41 (FFAR3) fatty acid receptor expression in human adipocytes: implications for the anti-inflammatory action of n-3 fatty acids. Arch. Physiol. Biochem. 124, 97–108. 10.1080/13813455.2017.1364774. [PubMed: 28835131]

81. Widmayer P, Kusumakshi S, Hägele FA, Boehm U, and Breer H (2017). Expression of the Fatty Acid Receptors GPR84 and GPR120 and Cytodifferentiation of Epithelial Cells in the Gastric Mucosa of Mouse Pups in the Course of Dietary Transition. Front. Physiol. 8, 601. 10.3389/fphys.2017.00601. [PubMed: 28871231]

82. Montgomery MK, Osborne B, Brandon AE, O'Reilly L, Fiveash CE, Brown SHJ, Wilkins BP, Samsudeen A, Yu J, Devanapalli B, et al. (2019). Regulation of mitochondrial metabolism in murine skeletal muscle by the medium-chain fatty acid receptor Gpr84. FASEB J 33, 12264–12276. 10.1096/fj.201900234R. [PubMed: 31415180]
83. Sun XN, An YA, Paschoal VA, de Souza CO, Wang MY, Vishvanath L, Bueno LM, Cobb AS, Nieto Carrion JA, Ibe ME, et al. (2023). GPR84-mediated signal transduction affects metabolic function by promoting brown adipocyte activity. J. Clin. Invest. 133, e168992. 10.1172/JCI168992. [PubMed: 37856216]
84. Xiao T, Yan Z, Xiao S, and Xia Y (2020). Proinflammatory cytokines regulate epidermal stem cells in wound epithelialization. Stem Cell Res. Ther. 11, 232. 10.1186/s13287-020-01755-y. [PubMed: 32527289]
85. Jiang Y, Tsoi LC, Billi AC, Ward NL, Harms PW, Zeng C, Maverakis E, Kahlenberg JM, and Gudjonsson JE (2020). Cytokinocytes: the diverse contribution of keratinocytes to immune responses in skin. JCI Insight 5, e142067. 10.1172/jci.insight.142067. [PubMed: 33055429]
86. Cooper PO, Haas MR, Noonepalle SKR, and Shook BA (2021). Dermal Drivers of Injury-Induced Inflammation: Contribution of Adipocytes and Fibroblasts. Int. J. Mol. Sci. 22, 1933. 10.3390/ijms22041933. [PubMed: 33669239]
87. Correa-Gallegos D, Ye H, Dasgupta B, Sardogan A, Kadri S, Kandi R, Dai R, Lin Y, Kopplin R, Shenai DS, et al. (2023). CD201. Nature 623, 792–802. 10.1038/s41586-023-06725-x. [PubMed: 37968392]
88. Venkataraman C, and Kuo F (2005). The G-protein coupled receptor, GPR84 regulates IL-4 production by T lymphocytes in response to CD3 crosslinking. Immunol. Lett. 101, 144–153. 10.1016/j.imlet.2005.05.010. [PubMed: 15993493]
89. Kim CH (2021). Control of lymphocyte functions by gut microbiota-derived short-chain fatty acids. Cell. Mol. Immunol. 18, 1161–1171. 10.1038/s41423-020-00625-0. [PubMed: 33850311]
90. Campoio TR, Oliveira FA, and Otton R (2011). Oxidative stress in human lymphocytes treated with fatty acid mixture: role of carotenoid astaxanthin. Toxicol. Vitro 25, 1448–1456. 10.1016/j.tiv.2011.04.018.
91. Hidalgo MA, Carretta MD, and Burgos RA (2021). Long Chain Fatty Acids as Modulators of Immune Cells Function: Contribution of FFA1 and FFA4 Receptors. Front. Physiol. 12, 668330. 10.3389/fphys.2021.668330. [PubMed: 34276398]
92. Buckley CD, Gilroy DW, and Serhan CN (2014). Proresolving lipid mediators and mechanisms in the resolution of acute inflammation. Immunity 40, 315–327. 10.1016/j.immuni.2014.02.009. [PubMed: 24656045]
93. Davis FM, denDekker A, Joshi AD, Wolf SJ, Audu C, Melvin WJ, Mangum K, Riordan MO, Kunkel SL, and Gallagher KA (2020). Palmitate-TLR4 signaling regulates the histone demethylase, JMJD3, in macrophages and impairs diabetic wound healing. Eur. J. Immunol. 50, 1929–1940. 10.1002/eji.202048651. [PubMed: 32662520]
94. Blad CC, Tang C, and Offermanns S (2012). G protein-coupled receptors for energy metabolites as new therapeutic targets. Nat. Rev. Drug Discov. 11, 603–619. 10.1038/nrd3777. [PubMed: 22790105]
95. Hirasawa A, Tsumaya K, Awaji T, Katsuma S, Adachi T, Yamada M, Sugimoto Y, Miyazaki S, and Tsujimoto G (2005). Free fatty acids regulate gut incretin glucagon-like peptide-1 secretion through GPR120. Nat. Med. 11, 90–94. 10.1038/nm1168. [PubMed: 15619630]
96. Itoh Y, Kawamata Y, Harada M, Kobayashi M, Fujii R, Fukusumi S, Ogi K, Hosoya M, Tanaka Y, Uejima H, et al. (2003). Free fatty acids regulate insulin secretion from pancreatic beta cells through GPR40. Nature 422, 173–176. 10.1038/nature01478. [PubMed: 12629551]
97. Yonezawa T, Kurata R, Yoshida K, Murayama MA, Cui X, and Hasegawa A (2013). Free fatty acids-sensing G protein-coupled receptors in drug targeting and therapeutics. Curr. Med. Chem. 20, 3855–3871. 10.2174/09298673113209990168. [PubMed: 23862620]
98. Li J, Ma A, Zhang R, Chen Y, Bolyard C, Zhao B, Wang C, Pich T, Li W, Sun N, et al. (2024). Targeting metabolic sensing switch GPR84 on macrophages for cancer immunotherapy. Cancer Immunol. Immunother. 73, 52. 10.1007/s00262-023-03603-3. [PubMed: 38349405]

99. Khalil N, Manganas H, Ryerson CJ, Shapera S, Cantin AM, Hernandez P, Turcotte EE, Parker JM, Moran JE, Albert GR, et al. (2019). Phase 2 clinical trial of PBI-4050 in patients with idiopathic pulmonary fibrosis. Eur. Respir. J. 53, 1800663. 10.1183/13993003.00663-2018. [PubMed: 30578394]

100. Strambu IR, Seemayer CA, Fagard LMCA, Ford PA, Van der Aa TAK, de Haas-Amatsaleh AA, Modgill V, Santermans E, Sondag EN, Helmer EG, et al. (2023). GLPG1205 for idiopathic pulmonary fibrosis: a phase 2 randomised placebo-controlled trial. Eur. Respir. J. 61, 2201794. 10.1183/13993003.01794-2022. [PubMed: 36328358]

101. Yang X, Zhang X, Heckmann BL, Lu X, and Liu J (2011). Relative contribution of adipose triglyceride lipase and hormone-sensitive lipase to tumor necrosis factor-α (TNF-α)-induced lipolysis in adipocytes. J. Biol. Chem. 286, 40477–40485. 10.1074/jbc.M111.257923. [PubMed: 21969372]

102. Liu D, Yang P, Gao M, Yu T, Shi Y, Zhang M, Yao M, Liu Y, and Zhang X (2019). NLRP3 activation induced by neutrophil extracellular traps sustains inflammatory response in the diabetic wound. Clin. Sci. 133, 565–582. 10.1042/CS20180600.

103. Serhan CN, Jain A, Marleau S, Clish C, Kantarci A, Behbehani B, Colgan SP, Stahl GL, Merched A, Petasis NA, et al. (2003). Reduced inflammation and tissue damage in transgenic rabbits overexpressing 15-lipoxygenase and endogenous anti-inflammatory lipid mediators. J. Immunol. 171, 6856–6865. 10.4049/jimmunol.171.12.6856. [PubMed: 14662892]

104. Haas MR, Nguyen DV, and Shook BA (2021). Recovery of Altered Diabetic Myofibroblast Heterogeneity and Gene Expression Are Associated with CD301b+ Macrophages. Biomedicines 9, 1752. 10.3390/biomedicines9121752. [PubMed: 34944568]

105. McGee HM, Schmidt BA, Booth CJ, Yancopoulos GD, Valenzuela DM, Murphy AJ, Stevens S, Flavell RA, and Horsley V (2013). IL-22 promotes fibroblast-mediated wound repair in the skin. J. Invest. Dermatol. 133, 1321–1329. 10.1038/jid.2012.463. [PubMed: 23223145]

Highlights

- Cutaneous *Gpr84* expression increases post-wounding
- Manipulation of GPR84 signaling alters myeloid cell numbers during injury-induced inflammation
- Inhibition of GPR84 signaling delays wound closure and revascularization
- Treating diabetic mouse wounds with decanoic acid rescues defects in inflammation and repair

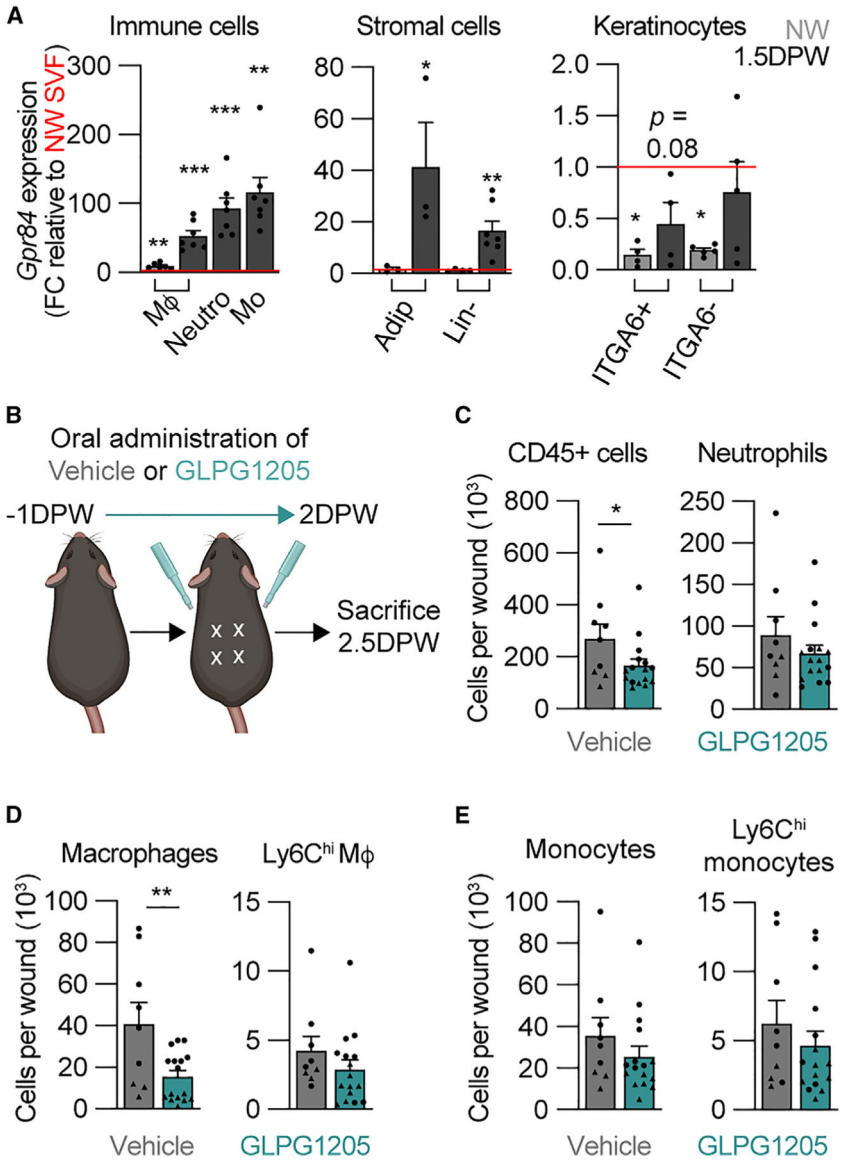

Figure 1. Inhibition of GPR84 reduces myeloid cell numbers during early inflammation

(A) Comparison of *Gpr84* expression in immune, stromal, and keratinocyte cells from NW and 1.5 DPW skin relative to NW stromal vascular fraction (SVF) ($n \geq 3$ male mice per condition). Significance was determined by one-way ANOVA prior to two-tailed Student's t test between the cell type of interest and the NW SVF.

(B) Schematic of the timeline of GLPG1205 treatment.

(C–E) Quantification from flow cytometry analysis of $SYTOX^-$ (C) immune cells ($CD45^+$) and neutrophils, (D) total wound macrophages and $Ly6C^{hi}$ macrophages, and (E) total monocytes and $Ly6C^{hi}$ monocytes in wound beds (WBs) 2.5 DPW ($n \geq 9$ mice, circles denote males and triangles denote females). Significance was determined by a two-tailed Student's t test.

Error bars indicate mean ± SEM. *$p < 0.05$, **$p < 0.01$, and ***$p < 0.001$. FC, fold change; M4, macrophage; Mo, monocyte; Neutro, neutrophil; Adip, adipocyte; Lin–, lineage-negative cells; NW, non-wounded; DPW, days post-wounding.

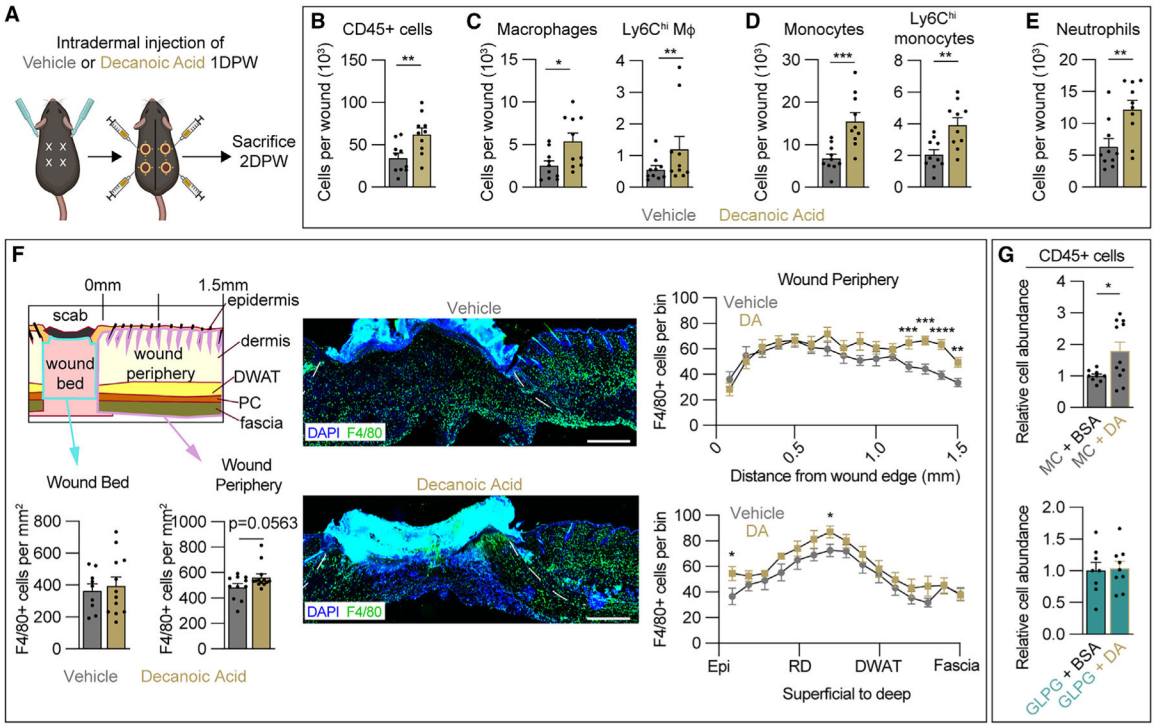

Figure 2. Injection of DA increases myeloid cell numbers during the inflammation phase of acute skin wound healing

(A) Schematic of decanoic acid (DA) treatment paradigm.

(B–E) Quantification from flow cytometry analysis of Zombie^{-} (B) CD45^{+} cells, (C) total wound macrophages and Ly6C^{hi} macrophages, (D) total monocytes and Ly6C^{hi} monocytes, and (E) neutrophils 2 DPW (n = 10 wounds from 5 male mice per condition).

(F) Spatial analysis of tissues immunostained for F4/80 to determine macrophage numbers in the wound bed (WB) and wound periphery (WP) of vehicle- and DA-treated animals. Dashed white lines delineate wound edges. Scale bars, 500 μm.

(G) Quantification from flow cytometry analysis of SYTOX^{-} CD45^{+} immune cells in methyl cellulose- (MC; top) or GLPG1205 (bottom)-treated mice injected intradermally at the WP with vehicle (BSA) or DA ($n \geq 11$ wounds for each condition in males).

Error bars indicate mean ± SEM. Significance was determined using a two-tailed Student's t test. *$p < 0.05$, **$p < 0.01$, ***$p < 0.001$, and ****$p < 0.0001$. M4, macrophage; DPW, days post-wounding; Epi, epidermis; RD, reticular dermis; DWAT, dermal white adipose tissue.

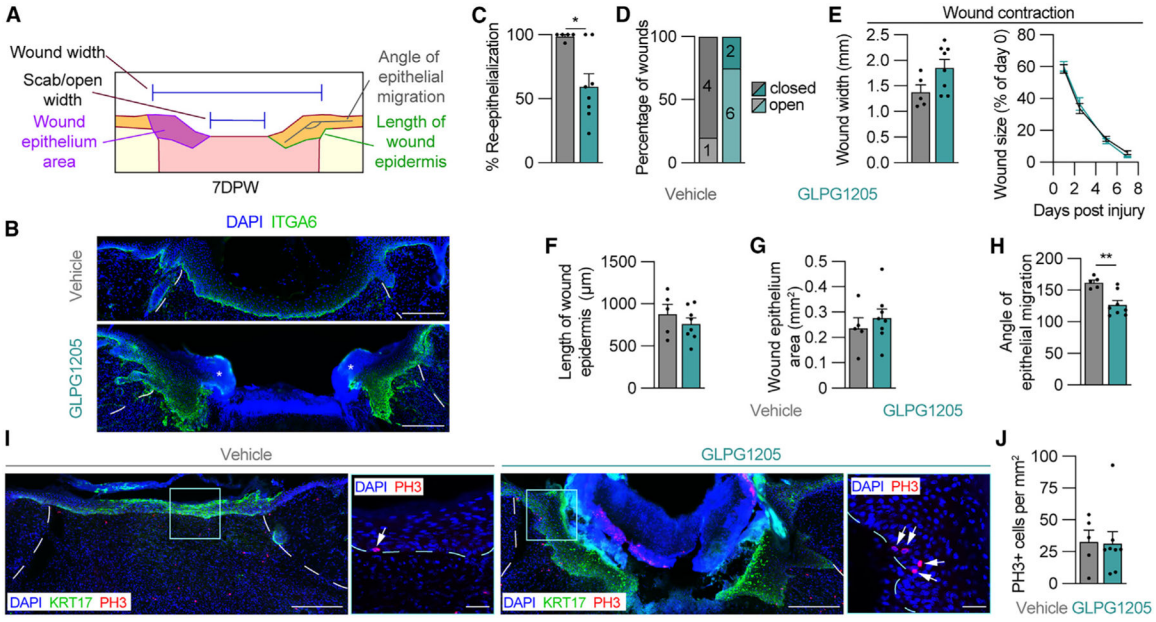

Figure 3. Inhibition of GPR84 signaling delays epidermal repair during skin wound healing

(A) Schematic of measurements used to assess the epithelium of wounds 7 DPW.

(B) ITGA6 immunostained tissue sections from the center of wounds obtained from vehicle- and GLPG1205-treated mice. Asterisks indicate scab.

(C–H) Quantification of parameters that assess epithelial repair including (C) WB re-epithelialization, (D) percentage of open versus closed wounds, (E) wound width and wound size, (F) length of wound epidermis, (G) wound epithelium area, and (H) the angle of epithelial migration. The angle of epithelial migration was measured on both sides of each section analyzed.

(I) Tissue immunostained for KRT17 and PH3. High-magnification images show PH3 in the epithelium. Arrows point to $PH3^+$ nuclei.

(J) Quantification of $PH3^+$ cells per area of wound epithelium ($n \geq 5$ wounds from ≥3 male mice per condition). Dashed white lines delineate wound edges, and dashed blue lines delineate epithelium. Scale bars, 250 μm in composite images and 25 μm in high-magnification images. Error bars indicate mean ± SEM. Significance was determined using a two-tailed Student's t test for all analyses except (D), where a Fisher's exact test was used. $*p < 0.05$ and $**p < 0.01$. KRT17, keratin 17; PH3, phospho-histone H3.

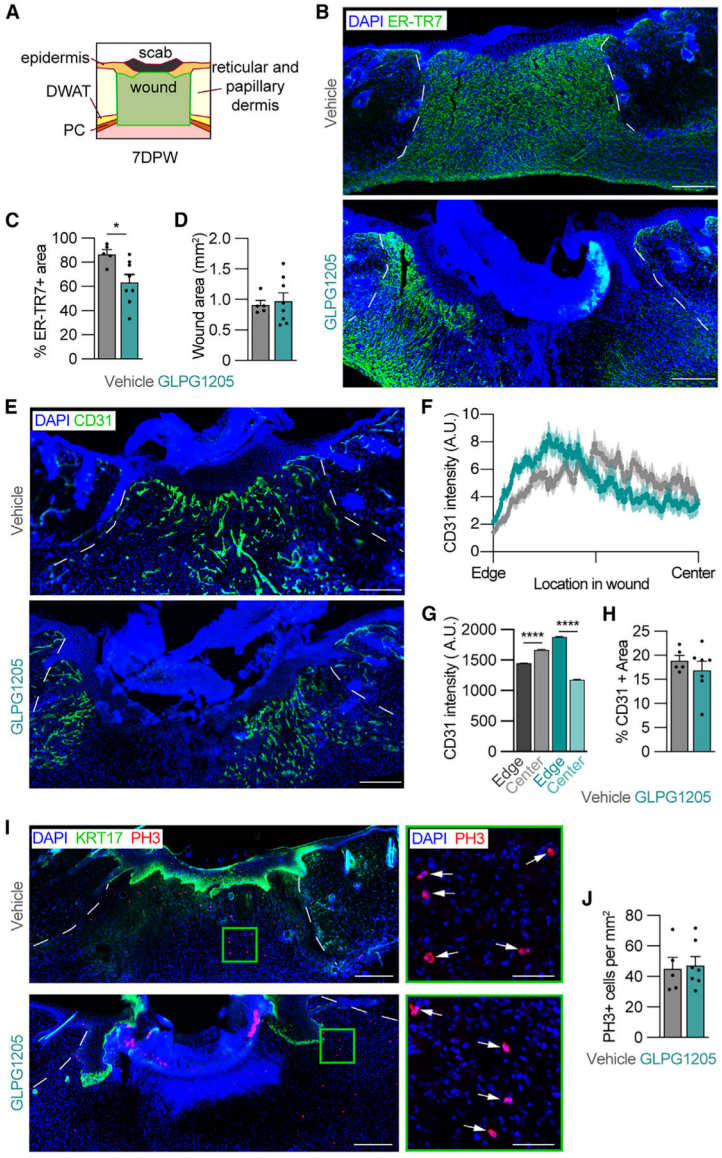

Figure 4. GPR84 contributes to dermal repair

(A) Schematic of the area analyzed to quantify the WB (outlined in green) 7 DPW.

(B) Images of 7 day wounds immunostained for ER-TR7 (fibroblasts) and quantification of (C) the percentage of ER-TR7$^+$ area and (D) total WB area. (E–H) 7 day wounds immunostained for CD31 (revascularization) (E) and corresponding quantification of the spatial distribution of CD31 mean fluorescence intensity from the wound edge to the center of the WB (F), the area under the curve for CD31 intensity in the edge and central regions of WBs (G), and the percentage of CD31$^+$ area (H) from vehicle- and GLPG1205-treated mice. The solid line and outer shading in (F) indicates mean ± SEM.

(I) Tissue sections from the center of wounds immunostained for KRT17 and PH3. High-magnification images (green boxes) show PH3 in WBs. Arrows indicate PH3$^+$ nuclei.

(J) Quantification of PH3$^+$ cells per area of WB ($n \geq 3$ male mice per condition). White lines delineate wound edges. Scale bars, 250 μm in composites and 50 μm for high-magnification

images. Error bars indicate mean ± SEM. Significance was determined by a two-tailed Student's t test. *$p < 0.05$ and ****$p < 0.0001$. DWAT, dermal white adipose tissue; PC, panniculus carnosus; A.U., arbitrary units of fluorescence; KRT17, keratin 17; PH3, phospho-histone H3.

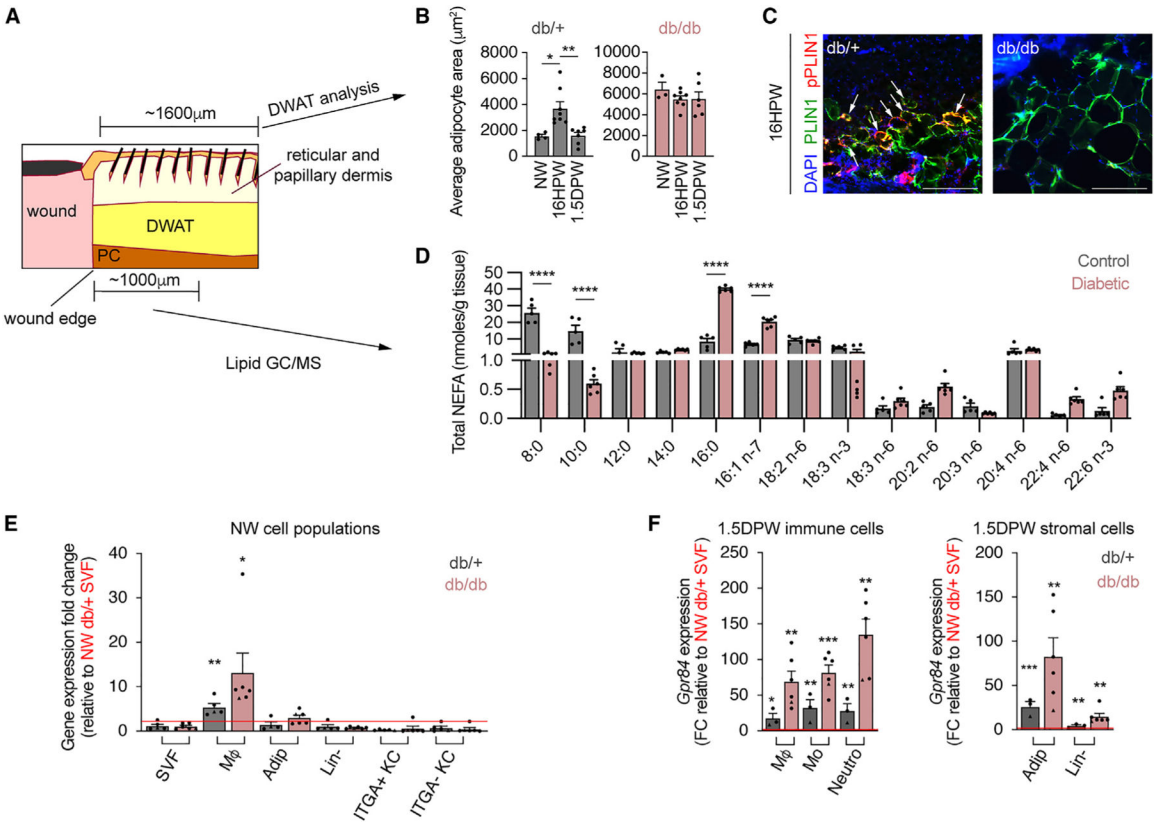

Figure 5. Changes in GPR84 signaling components in diabetic mouse skin wounds

(A) Schematic showing delineated DWAT and tissue components assessed by lipid GC/MS.

(B) Quantification of lean (db/+) and diabetic (db/db) adipocyte cross-sectional area between NW, 16 HPW, and 1.5 DPW time points.

(C) Images of db/+ and db/db and adipocytes from 16 HPW sections immunostained for PLIN1 and pPLIN1 ($n \geq 3$ male mice per condition). Scale bars, 250 μm.

(D) Lipid MS/MS quantification of total NEFAs detected in 1 DPW WP of lean control and diabetic mice ($n \geq 5$ male mice per condition).

(E and F) Quantitative RT-PCR analysis of *Gpr84* expression in cells isolated from NW (E) and 1.5 DPW (F) db/+ and db/db skin by fluorescence-activated cell sorting ($n \geq 3$ mice, circles denote males and triangles denote females).

Error bars indicate mean ± SEM. Significance was determined for (B) using a one-way ANOVA followed by a two-tailed Student's t test, for (D) using two-way ANOVA with Šidák correction, and for (E) using a two-tailed Student's t test. *$p < 0.05$, **$p < 0.01$, ***$p < 0.001$, and ****$p < 0.0001$. DWAT, dermal white adipose tissue; NW, non-wounded; HPW, hours post-wounding; DPW, days post-wounding; PLIN1, Perilipin 1; NEFA, non-esterified fatty acids; PC, panniculus carnosus; FC, fold change; SVF, stromal vascular fraction.

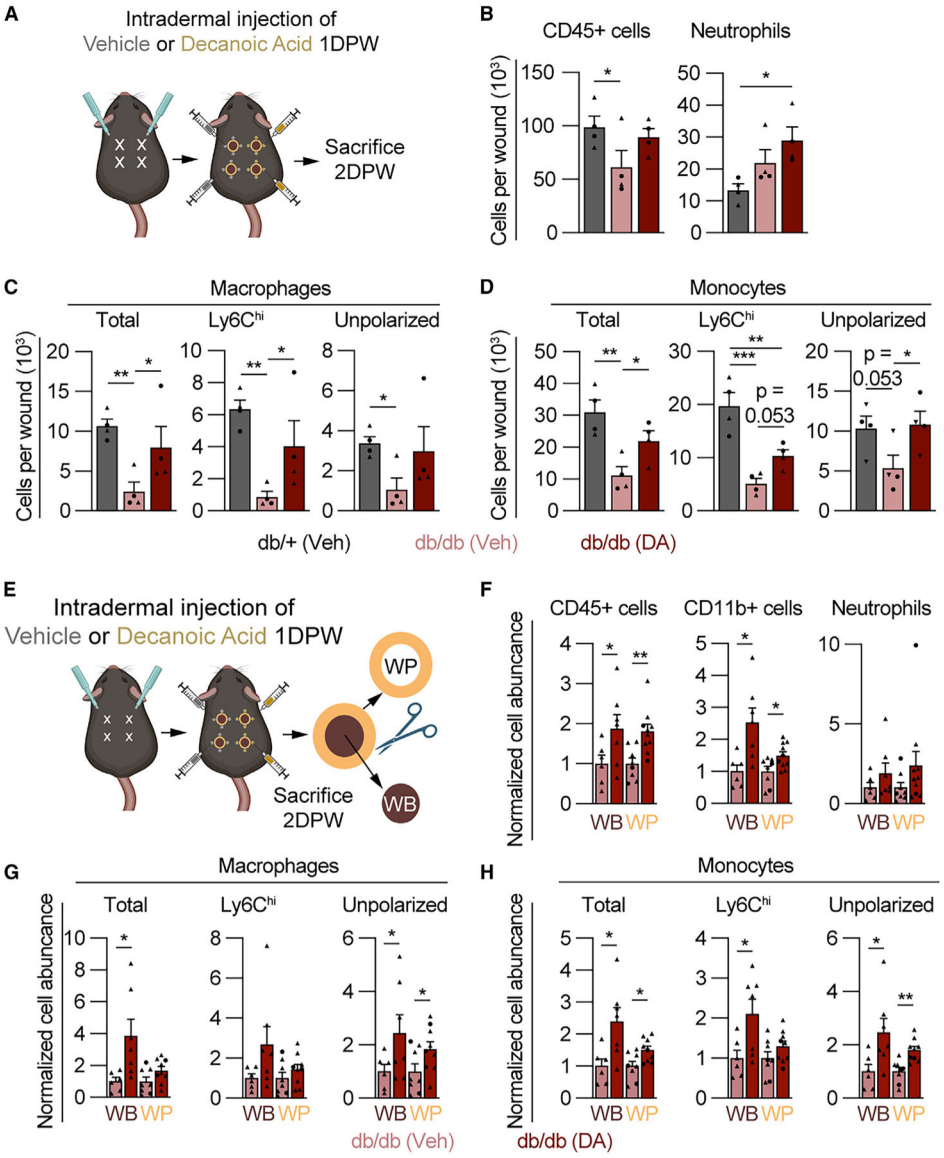

Figure 6. DA increases myeloid cell numbers 2 DPW in diabetic mice

(A) Schematic showing the timeline for DA treatment and myeloid cell analysis.

(B–D) Quantification of flow cytometry for SYTOX^{-} (B) CD45^{+} cells and neutrophils, (C) macrophages (total, Ly6C^{hi}, and unpolarized), and (D) monocytes (total, Ly6C^{hi}, and unpolarized) 2 DPW in db/+ mice treated with vehicle and db/db mice treated with vehicle or DA (n = 4 mice, circles denote males and triangles denote females). Significance was determined in (B)–(D) by one-way ANOVA corrected for multiple comparisons using the two-stage setup method of Benjamini, Krieger, and Yekutieli.

(E–H) Schematic showing the procedure for separation of WB from WP, for flow cytometry analysis of SYTOX^{-} (F) CD45^{+} cells, myeloid cells (CD11b^{+}), and neutrophils, (G) macrophage subsets, and (H) monocytes ($n \geq 9$ wounds per condition, circles denote males and triangles denote females). Significance was determined by a two-tailed Student's t test.

Error bars indicate mean ± SEM. *$p < 0.05$, **$p < 0.01$, and ***$p < 0.001$. M4, macrophage; DPW, days post-wounding; DA, decanoic acid.

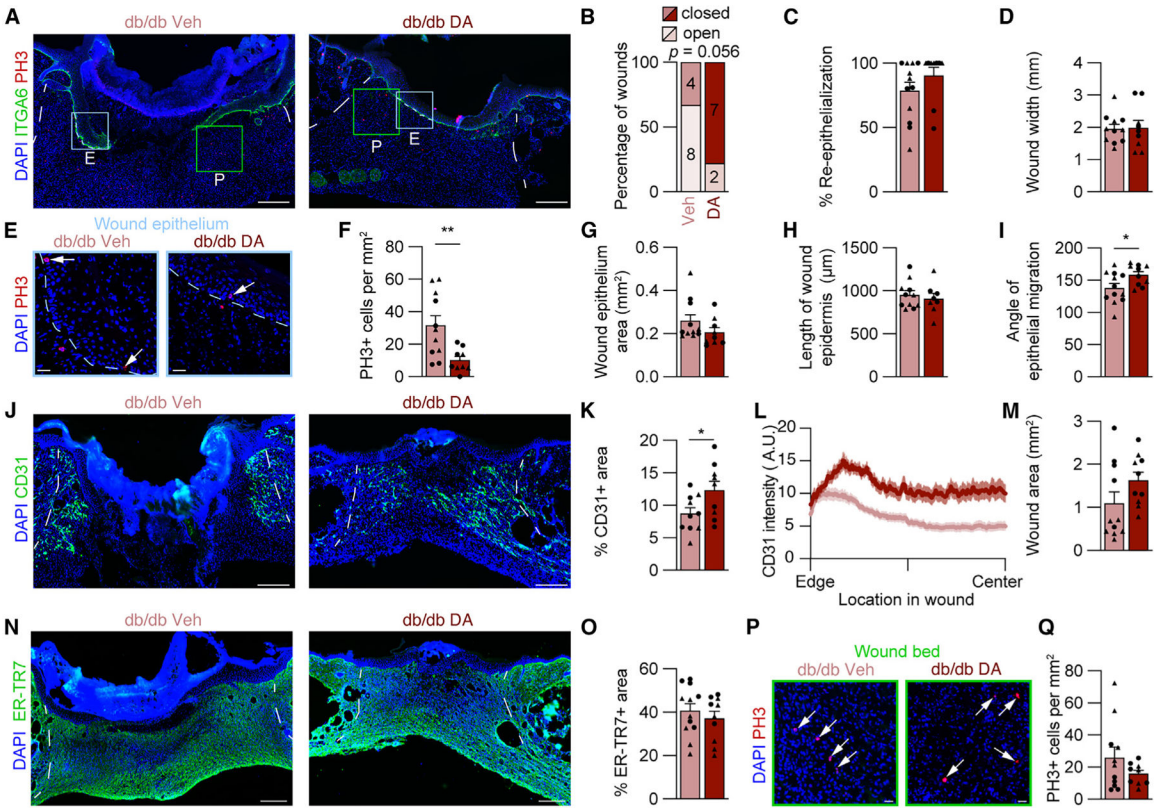

Figure 7. DA treatment improves diabetic wound healing

(A) Composite images of 7 DPW tissue sections from vehicle- and DA-treated db/db mouse wounds immunostained for ITGA6 and PH3. Boxes indicating high-magnification areas shown in (E) and (P), and blue and green boxes indicate regions in epithelial and WB images, respectively.

(B–D) Corresponding quantification of (B) the percentage of open versus closed wounds, (C) percentage of re-epithelialization, and (D) wound width.

(E) High-magnification images from (A) showing PH3 in the wound epithelium. Arrows indicate $PH3^+$ nuclei.

(F) Quantification of $PH3^+$ cells per area of wound epithelium.

(G–I) Quantitative comparison of (G) wound epithelium area, (H) length of wound epidermis, and (I) angle of epithelial migration at the center of WBs. The angle of epithelial migration was measured on both sides of each section analyzed.

(J–M) Images of 7 DPW sections immunostained for CD31 (J) and quantifications of percentage of $CD31^+$ area (K), CD31 average spatial intensity from wound edge to center (L), and wound area (M). The solid line and outer shading in (L) indicates mean ± SEM.

(N and O) Images from immunostained tissue sections for ER-TR7 (N) and quantification of the percentage of ER-TR7+ area (O).

(P and Q) High-magnification area showing $PH3^+$ cells in the WB (arrows indicate $PH3^+$ nuclei) (P) and $PH3^+$ cells per area of WB (Q) ($n \geq 5$ mice per condition, circles denote males and triangles denote females).

Blue dotted lines delineate wound epithelium, and white lines delineate wound edges. Scale bars, 250 μm for low-magnification composite images and 25 μm for high-magnification

images. Error bars indicate mean ± SEM. Significance was determined using a two-tailed Student's t test for all analyses except (B), where a Fisher's exact test was used. *$p < 0.05$ and **$p < 0.01$. DPW, days post-wounding; A.U., arbitrary units of fluorescence; ITGA6, integrin 6a; PH3, phospho-histone H3; DA, decanoic acid; A.U., arbitrary units.

KEY RESOURCES TABLE

REAGENT or RESOURCE	SOURCE	IDENTIFIER
Antibodies		
APC/Cy7 anti-mouse CD45 rat monoclonal (Clone 30-F11)	Biolegend	Cat# 103116; RRID: AB_312981
Alexa Fluor 700 anti-mouse CD11b rat monoclonal (Clone M1/70)	Biolegend	Cat# 101222; RRID: AB_493705
eFluor 450 anti-mouse F4/80 rat monoclonal (Clone BM8)	eBioscience	Cat# 48-4801-82; RRID: AB_1548747
BV785 anti-mouse Ly6G rat monoclonal (clone 1A8)	Biolegend	Cat# 127645; RRID: AB_2566317
BV570 anti-mouse Ly6C rat monoclonal (clone HK1.4)	Biolegend	Cat# 128030; RRID: AB_2562617
Alexa Fluor BV650 anti-mouse CD206 rat monoclonal (clone C068C2)	Biolegend	Cat# 141723; RRID: AB_2562445
APC-Fire750 anti-mouse CD31 rat monoclonal (clone 390)	Biolegend	Cat# 102434; RRID: AB_2629683
APC anti-mouse EpCAM (clone G8.8)	Biolegend	Cat# 118214; RRID: AB_1134102
BV650 anti-mouse CD49f (clone GoH3)	BD Biosciences	Cat# 563707; RRID: AB_2744415 https://www.antibodyregistry.org/AB_2744415
Anti-CD31 rat monoclonal (clone MEC13.3)	BD Biosciences	Cat# 550274; RRID: AB_393571
Anti-CD68 rabbit polyclonal	Abcam	Cat# ab125212; RRID: AB_10975465
Anti-ER-TR7 rat monoclonal	Abcam	Cat# ab51824; RRID: AB_881651
Anti-F4/80 rat monoclonal (clone CI:A3-1)	Abcam	Cat# ab6640; RRID: AB_1140040
Anti-ITGA6 rat monoclonal (clone GoH3)	R&D Systems	Cat# MAB13501; RRID: AB_2128311
Anti-Keratin 17 rat monoclonal (clone W1613A)	Biolegend	Cat# 697202; RRID: AB_2687136
Anti-Perilipin1 goat polyclonal	Abcam	Cat# ab61682; RRID: AB_944751
Anti-phospho-Histone H3	Abcam	Cat# ab5176; RRID: AB_304763
Anti-phospho-Perilipin1 (S497)	Vala Sciences	Cat# 4855
Chemicals, peptides, and recombinant proteins		
Decanoic Acid	Sigma	C1875
Liberase TM	Roche	05401127001
SYTOX Green and Orange	Invitrogen	S34860, S34861
Zombie Aqua	Biolegend	423102
GLPG1205	Galapagos Pharmaceuticals	GLPG1205
6-(octylamino)-2,4(1H,3H)-pyrimidinedione (6-OAU)	Cayman Chemical	17687
Lipopolysaccharides from *E. coli* (LPS)	Sigma	L4391
TRIzol	Invitrogen	15596018
Critical commercial assays		
RNeasy Plus Micro Kit	Qiagen	74034
SuperScript IV First-Strand Synthesis System	Invitrogen	180901050
Experimental models: Organisms/strains		
Mouse: C57BL/6	The Jackson Laboratory	000664
Mouse: B6.BKS(D)-Leprdb/J	The Jackson Laboratory	000697

REAGENT or RESOURCE	SOURCE	IDENTIFIER
Oligonucleotides		
PCR primers, see Table S1	This study	N/A
Software and algorithms		
Fiji (ImageJ)	NIH	https://fiji.sc
Adobe Photoshop	Adobe	https://www.adobe.com/products/photoshop.html
FlowJo	FlowJo, LLC	https://www.flowjo.com
MATLAB	MathWorks	https://www.mathworks.com
GraphPad Prism	GraphPad Software, Inc	https://www.graphpad.com